Annual Report –
Center for Space Telemetering and Telecommunications Systems
New Mexico State University

by
Stephen Horan, Phillip DeLeon, Deva Borah,
and Ray Lyman

NMSU-ECE-02-001

Annual Report – Center for Space Telemetering and Telecommunications Systems New Mexico State University

Stephen Horan, Phillip DeLeon, Deva Borah,
and Ray Lyman

Manuel Lujan Space Tele-Engineering Program
New Mexico State University

Prepared for

NASA Goddard Space Flight Center
Greenbelt, MD

under Grant NAG5-9323

March 18, 2002

Klipsch School of Electrical and Computer Engineering
New Mexico State University
Box 30001, MSC 3-O
Las Cruces, NM 88003-8001

Annual Report – Center for Space Telemetering and Telecommunications Systems New Mexico State University

Stephen Horan

Phillip DeLeon

Deva Borah

Ray Lyman

Contents

- NMSU Support
- Degree Production
- Small Satellite Communications
- Bandwidth Efficient Modulation
- ISI Compensation
- Space Internet Communications
- Optical Communications
- Adaptive Spread Spectrum Receivers

NMSU Support

- During the summer of 2001, the faculty and students moved from the Thomas & Brown Electrical & Computer Engineering building to the newly-remodeled Goddard Annex.
- 13000 ft^2 research facility. About ½ the space is for communications, signal processing, and telemetry research and ½ for photonics research

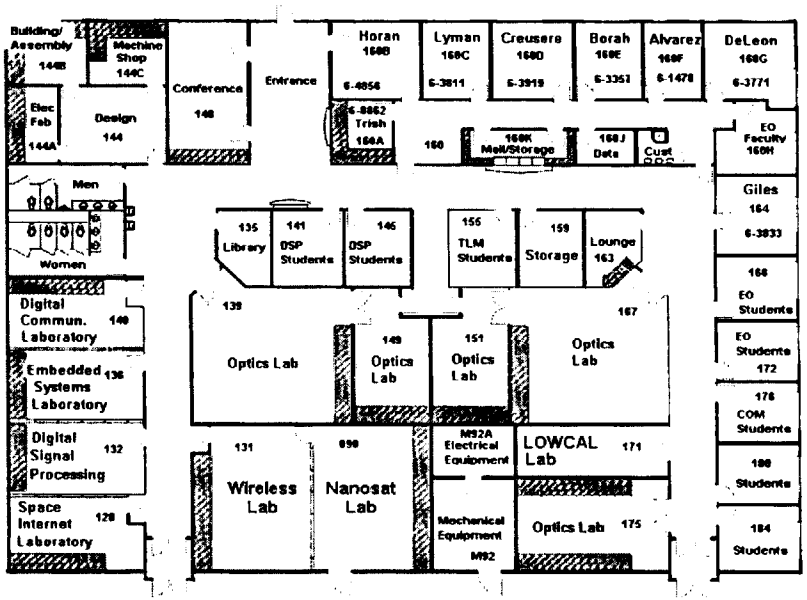

Degree Production

- PhD degrees awarded based on NASA research
  - Stephan Berner and Ru-hai Wang
- MSEE degrees awarded based on NASA research
  - John MacConnell, Christopher Garrett, Q. Zhao, Phillip Stanley
- MSEE degrees expected by the end of the summer
  - Anirban Chakraborti, Sandeep Mudassami

Small Satellite Communications

Stephen Horan

Klipsch School of Electrical and Computer Engineering

New Mexico State University

Contents

- Nanosatellite Radio Development
- Ground Communications Network
- Virtual Satellite Development

Nanosatellite Radio Development

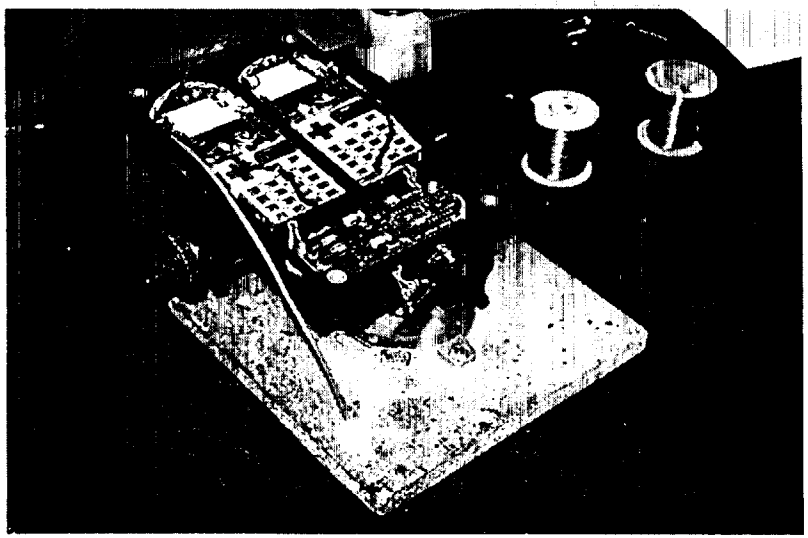

COTS-based radio system for the 3 Corner Satellite formation modified for flight constraints.

- Developed a flight radio system for the 3 Corner Satellite cluster of three nanosatellites
  - VHF Telemetry
  - UHF Command
  - UHF Inter-satellite

Nanosatellite Radio Development

- Performed
  - Hitchhiker Vibration Qualification Testing
  - Thermal Testing
- Participated in Phase 0/1 Safety Review at Johnson Space Center

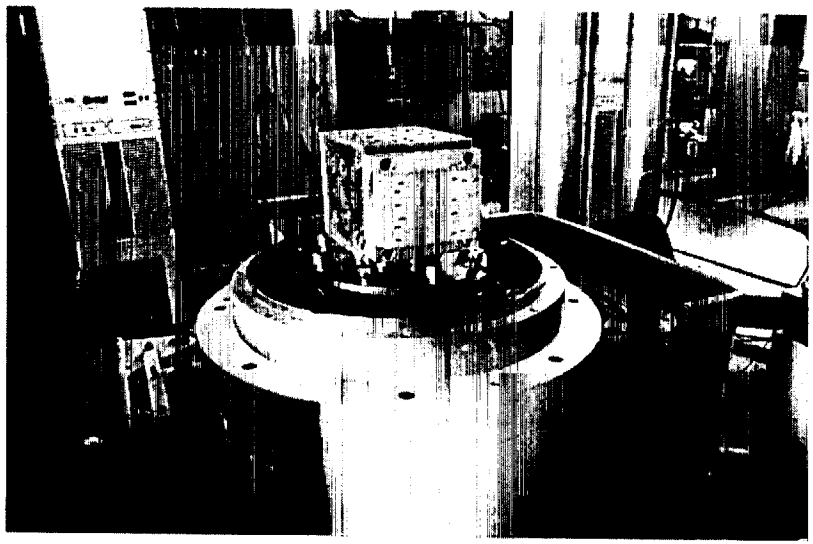

Radio undergoing vibration testing

Nanosatellite Radio Development

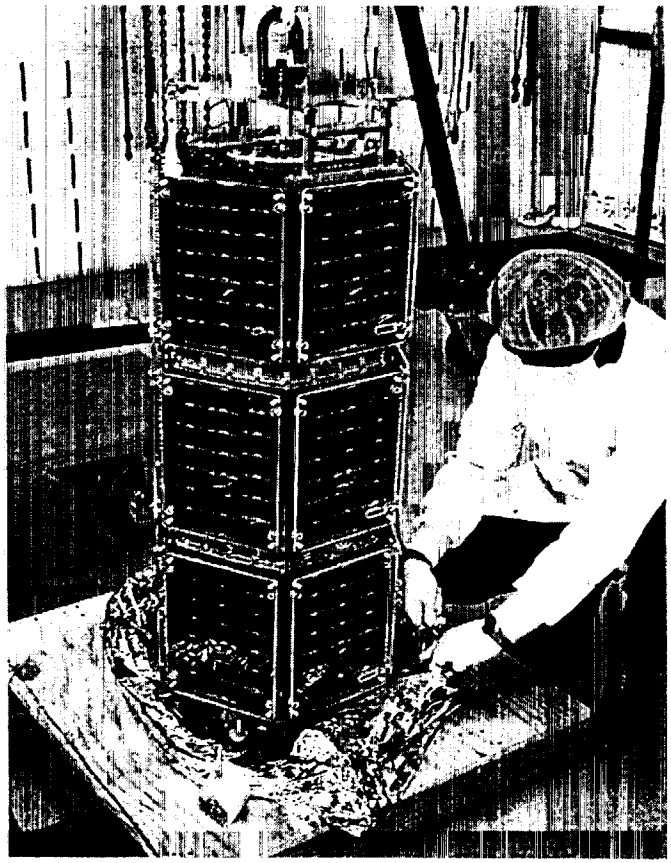

- Cluster of three nanosatellites delivered to the Air Force for integrated testing and preparation for flight on Shuttle in 2003

Ground Communications Network

- Developing a means to connect the three universities in the 3 Corner Satellite formation to share command and telemetry functions
- Allows for a central control and multiple support ground stations
- Uses LabVIEW modules communicating over the Internet
  - Real-time command and telemetry links
  - Store-and-forward command and telemetry capabilities
  - Automatic control of ground tracking hardware
  - Security & status

Virtual Satellite Development

- Goal is to develop S-Band RF test capability for data communications to complement simulation capability
  - Have gotten the NMSU antenna design class to produce TDRS-MA compatible antennas
  - Currently integrating antennas with Microdyne Telemetry Simulator for RF transmission and Telemetry Receiver for RF reception

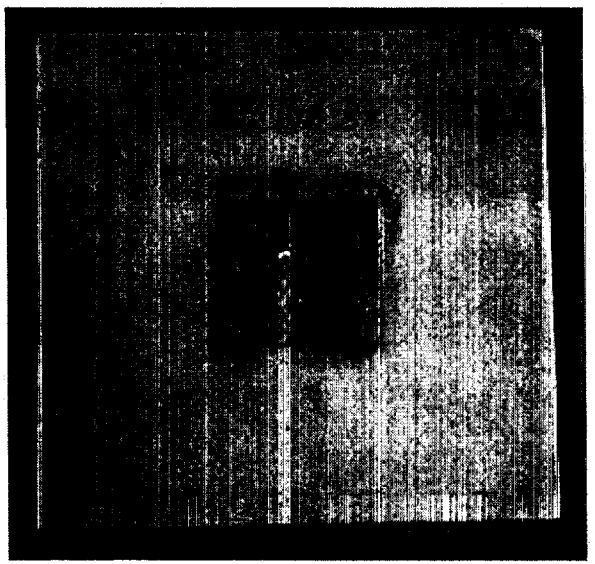

TDRSS-MA compatible Patch antenna developed by the antenna design class

Virtual Satellite Development

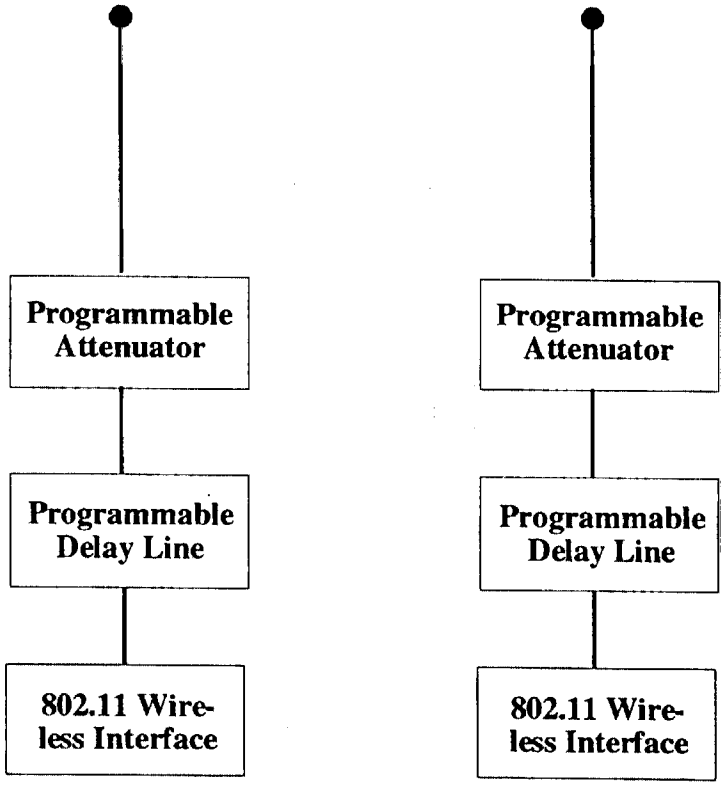

- Investigating a concept for virtual formation studies
  - Use Wireless LAN standards, e.g. 802.11
  - Add programmable delay and attenuation to model orbital effects
- Would permit studies of formation flying communications

Modulation and Detection Studies

Presented by

Dr. Deva K. Borah

Assistant Professor,
Klipsch School of Electrical and Computer Engineering,
New Mexico State University, Las Cruces, NM 88003, USA

OVERVIEW

- Research Publications

Part 1

- Introduction to Smooth Phase Interpolated Keying (SPIK)
- Bandwidth and Power Efficiency Results

Part2

- Introduction to Multiuser CDMA
- Turbo Detection/Decoding Results
- Future Work

Research Publications

- D. K. Borah and S. Horan, "Detection Techniques for Enhanced FQPSK Signals," IEEE GLOBECOM'2001, San Antonio, USA, Nov. 2001.
- Q. Zhao and D. K. Borah "Adaptive Iterative CDMA Multiuser Detection in Unknown Multipath Channels," to appear in IEEE ICC'2002, New York, April 2002.
- D. K. Borah and S. Horan, "EFQPSK versus CERN: A Comparative Study," Technical Report, NMSU-ECE-01-014, Sept. 2001.
- Q. Zhao, "Adaptive Iterative CDMA Multiuser Detection," Masters Thesis, Dec. 2001.

PART I

To study a constant envelope modulation technique, called the smooth phase interpolated keying (SPIK), and to compare its performance with other modulation techniques.

Communication System

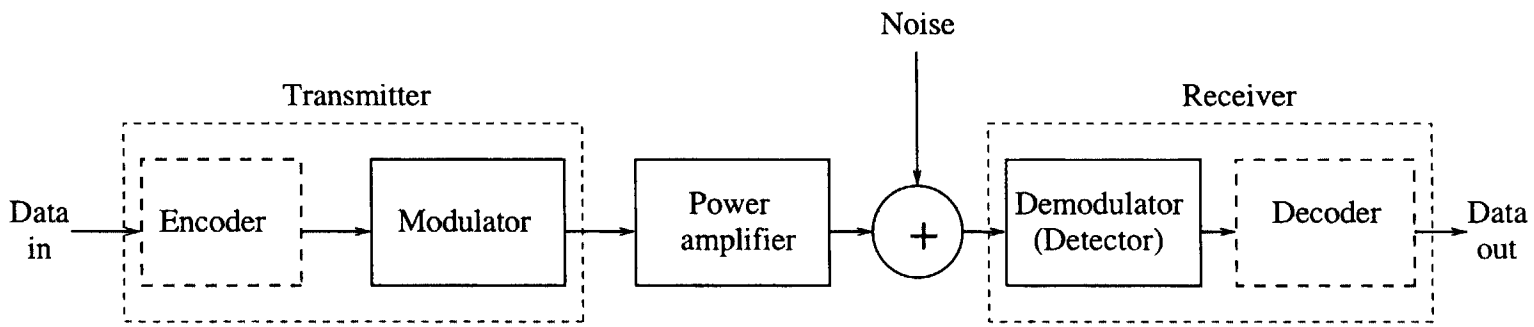

Smooth Phase Interpolated Keying (SPIK) Block Diagram

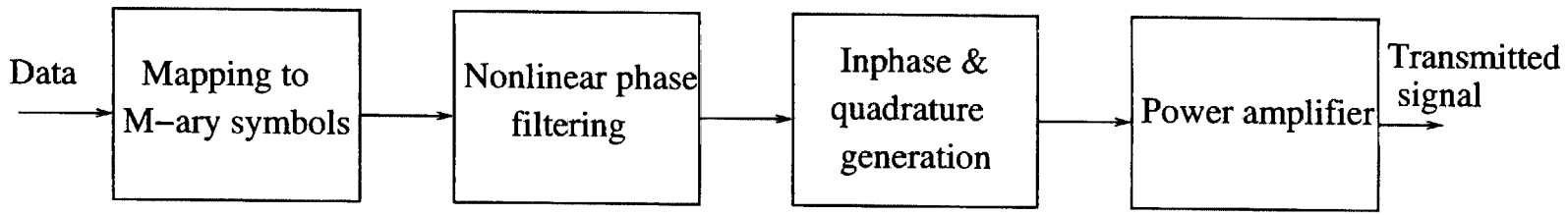

Spectra: SPIK vs. GMSK (BT=0.3)

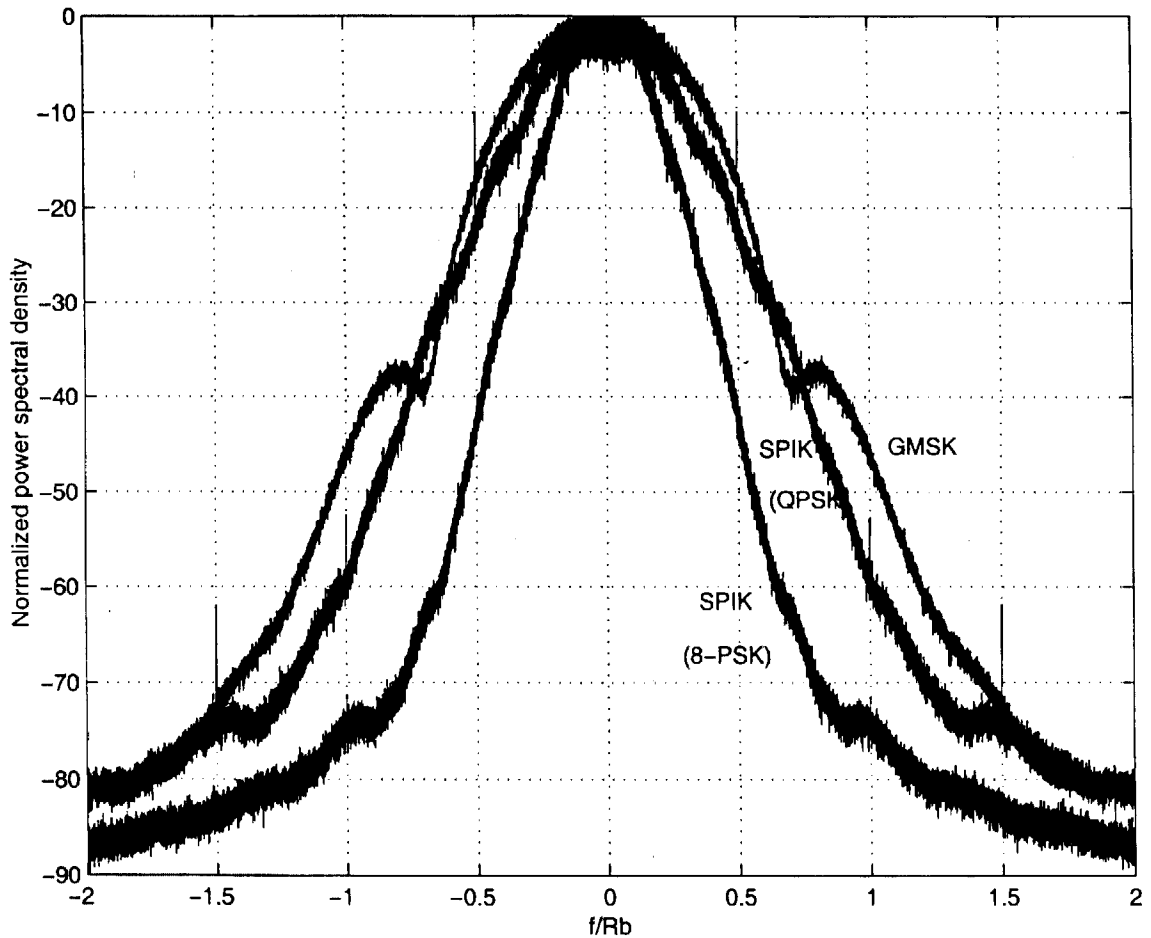

Spectra: SPIK vs. EFQPSK

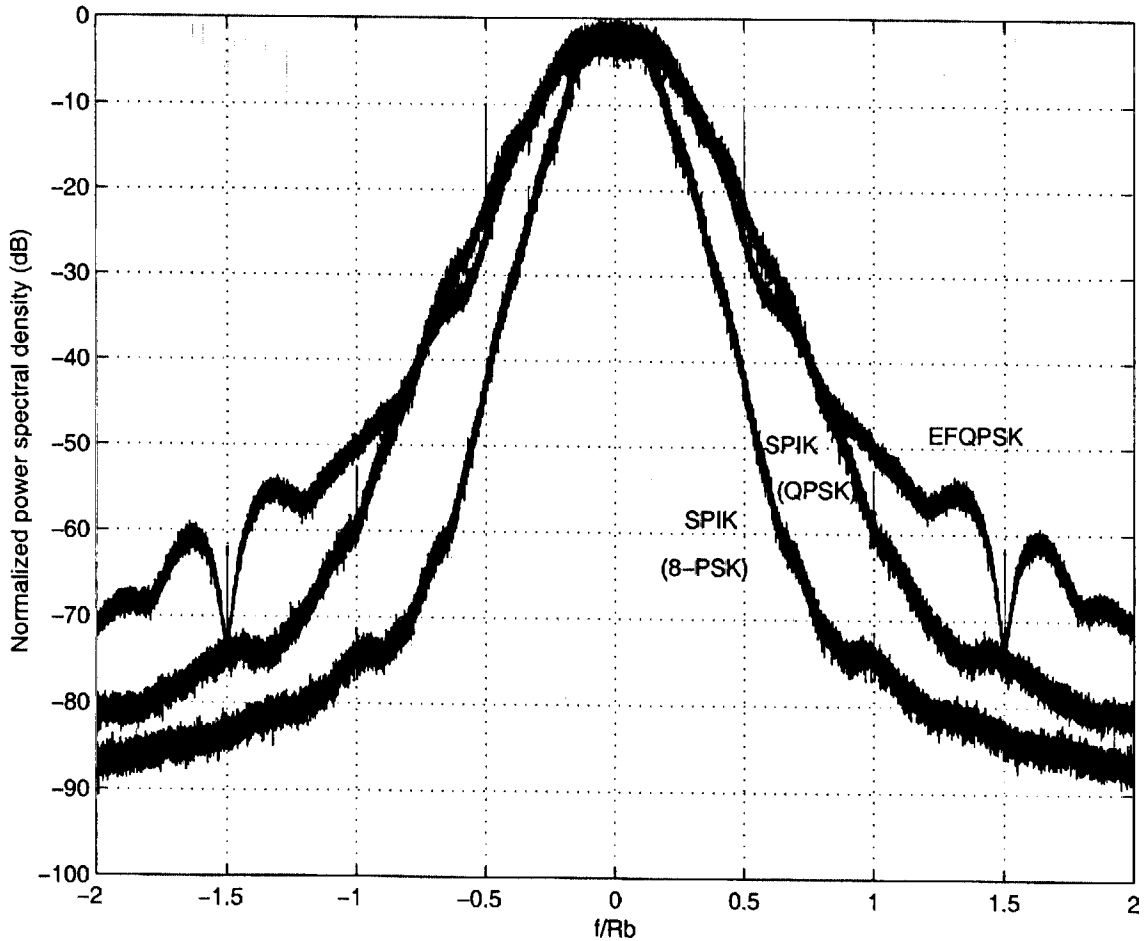

Spectra: SPIK ($\pi/4$-QPSK) vs. GMSK(BT=0.3)

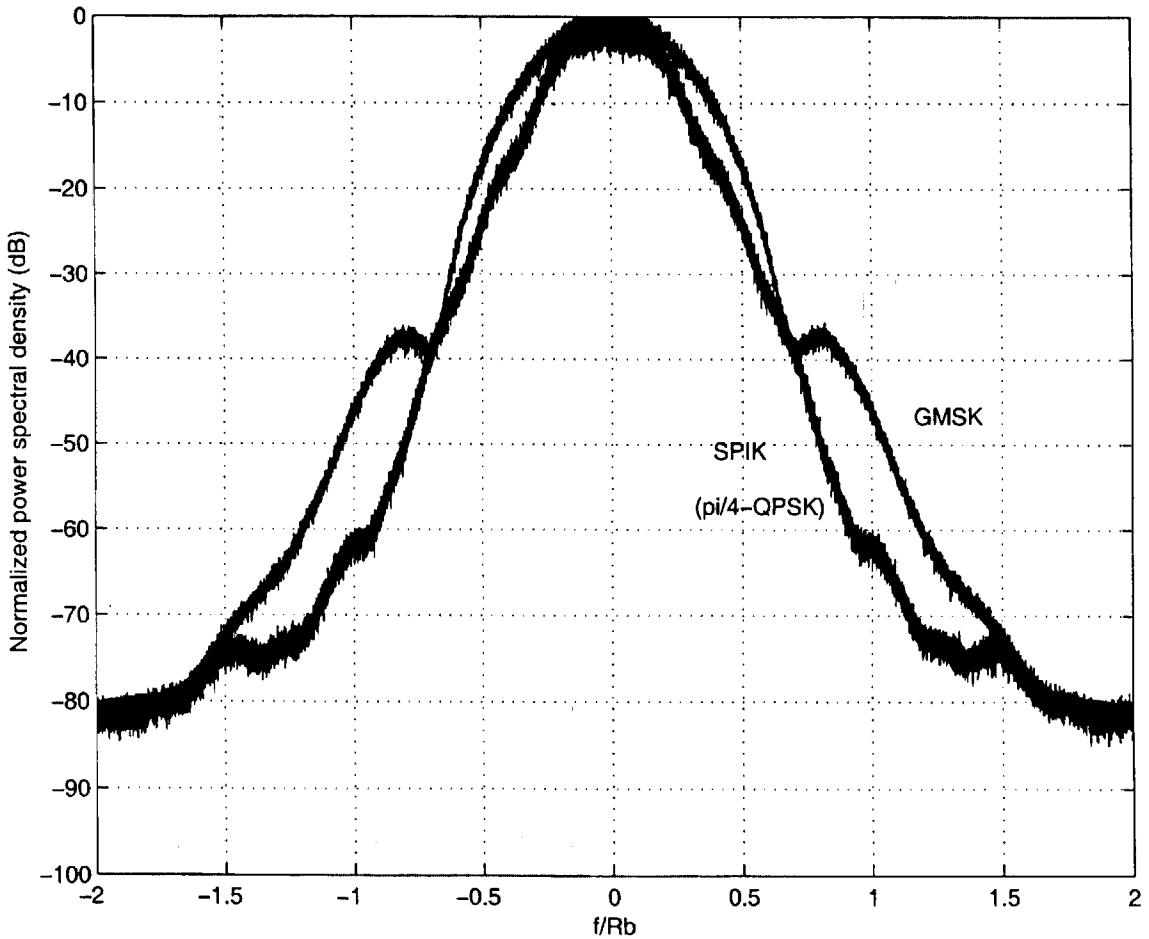

Spectra: SPIK ($\pi/4$-QPSK) vs. EFQPSK

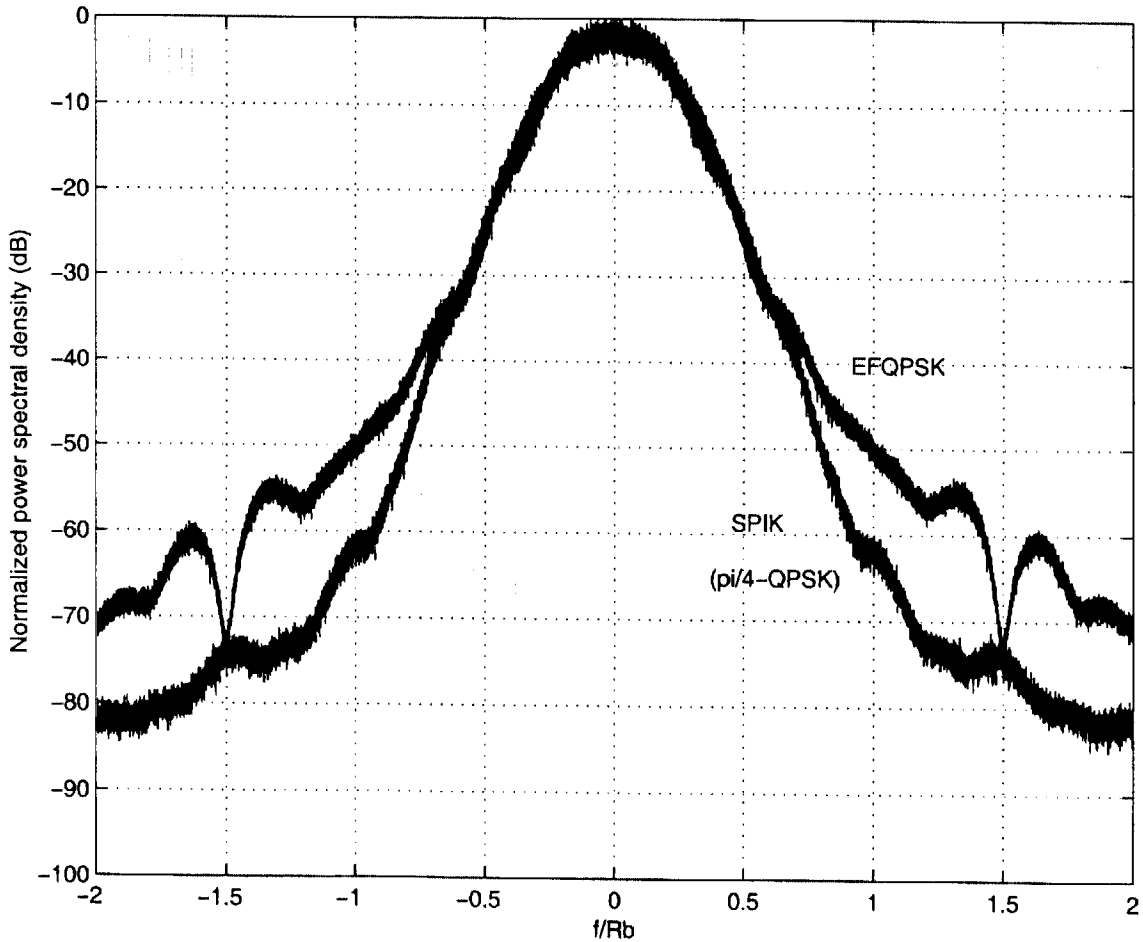

Comments on SPIK spectra

- SPIK is a constant envelope modulation technique and it is suitable for power efficient nonlinear amplification without spectral side lobe regeneration.
- SPIK with QPSK-type modulation performs better than Enhanced Feher's QPSK and GMSK with BT=0.3.
- Spectral lines are observed for QPSK. However, they disappear for $\pi/4$ QPSK and 8 PSK. This needs more investigation.

BER Performance of SPIK

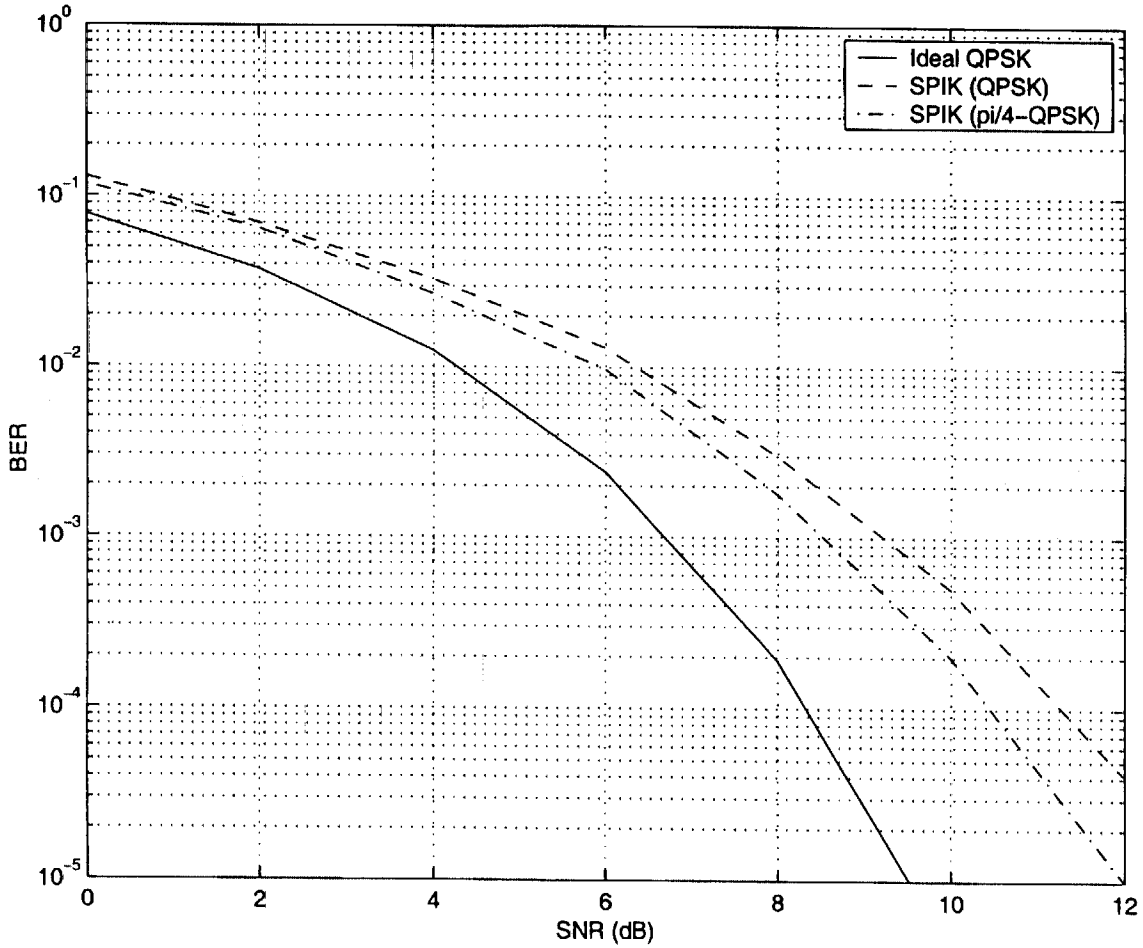

BER Performance of SPIK (TCM 8PSK)

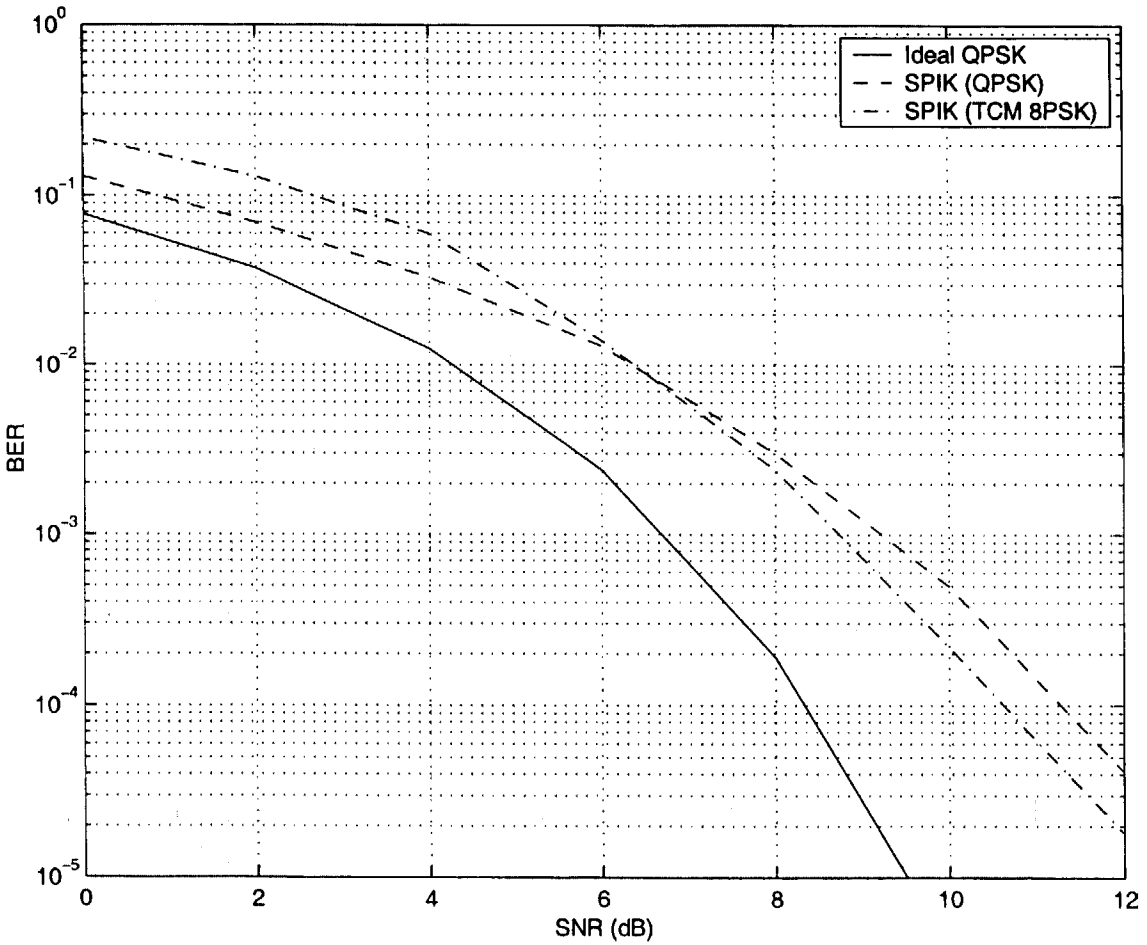

Comments on BER Performance of SPIK

- BER of SPIK (QPSK) is about 3 dB worse compared to ideal QPSK at 10^{-4}. However, BER of SPIK ($\pi/4$-QPSK) is only 2 dB worse compared to ideal QPSK.
- A simple 4-state 8PSK TCM shows only about 0.5 dB improvement over SPIK (QPSK) at a BER of 10^{-4}. Hence, there is a need to explore this further to see how more gain can be achieved, possibly using an equalizer.
- Since the above SPIK receivers considered only employ a 4-th order Butterworth filter with threshold detection, there is a need to investigate more sophisticated detectors that exploit the inherent memory in the modulation.

Future Directions

- Explore the use of an equalizer and investigate if this can improve TCM SPIK performance. Investigate the use of more sophisticated coding.
- Study the BER performance of SPIK for Ka band (in consultation with NASA GSFC) and compare with other modulation techniques.
- Study adaptive modulation for Ka band (in consultation with NASA GSFC).
- Investigate higher order modulation and performance with coding for SPIK. Explore improving SPIK's performance using the inherent memory of the modulation.

PART II

To study an adaptive turbo multiuser receiver that can suppress interference from undesired interferers.

Adaptive turbo multiuser detector structure

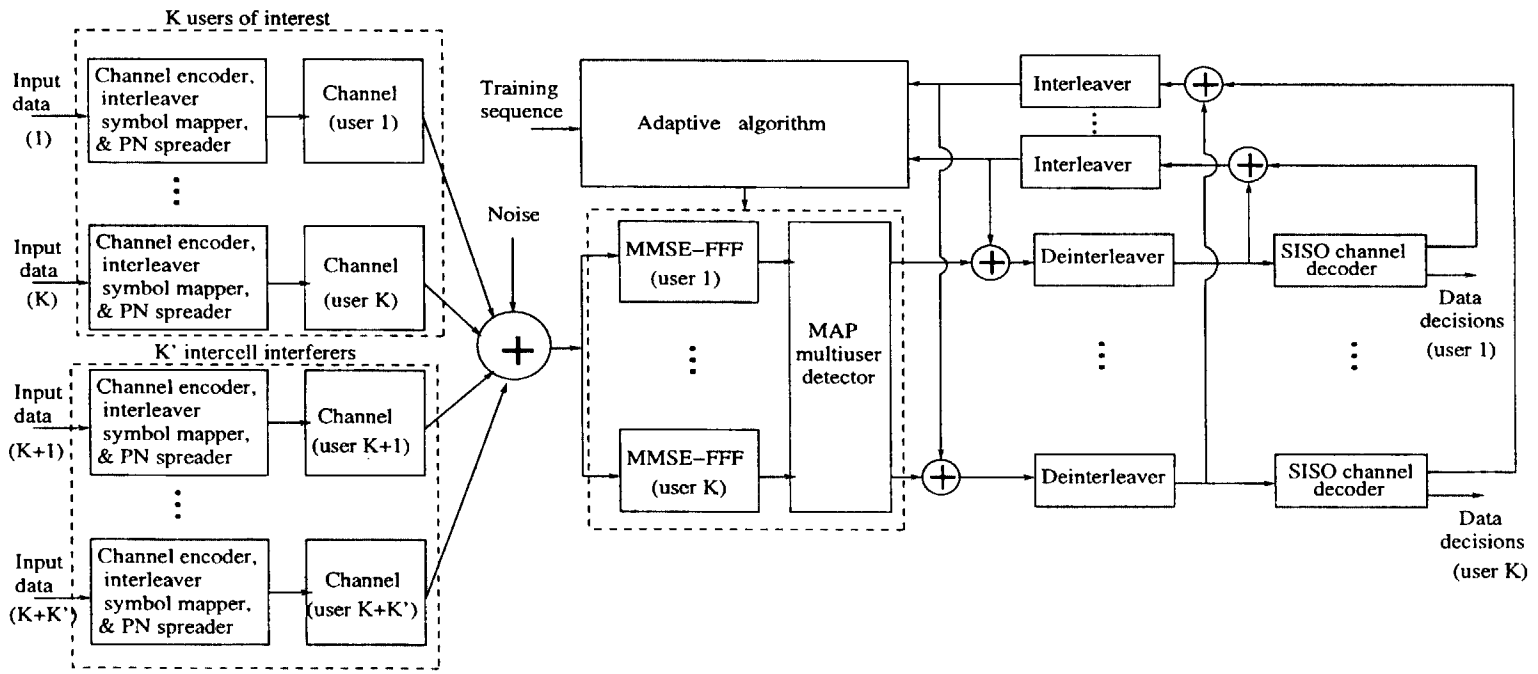

Signal Model

The received signal is modeled as

$$y(t) = \sum_{k=1}^{K+K'} \sum_{i=0}^{N_b-1} b_{k,i} s_k(t - iT - \tau_k) + n(t)$$

where

- $b_{k,i}$ is the i-th bit of the k-th user.
- K and K' are respectively the number of desired and undesired users.
- $s_k(t)$ is spreading waveform.
- N_b is the number of bits from each user, and $n(t)$ is noise.
- T is bit period and τ_k is arbitrary delay.

Highlights of adaptive turbo multiuser detector

- The receiver consists of a MAP multiuser detector and a bank of soft input soft output (SISO) channel decoders, with one decoder for each user.
- The MAP multiuser detector employs a bank of linear filters and a set of feedback coefficients, representing interference from different users. The linear filters and the decision coefficients are obtained adaptively without any *a priori* knowledge about the spreading sequences and their exact timings.
- The receiver can suppress undesired interferers.

MAP multiuser detector

- The MAP multiuser detector delivers *a posteriori* log-likelihood ratios (LLR)

$$\Lambda(b_{k,i}) = \log \frac{P[b_{k,i} = +1|\mathbf{y}]}{P[b_{k,i} = -1|\mathbf{y}]}$$

  where $\mathbf{y}$ is the received signal vector.

- All the necessary parameters are obtained adaptively, and the BCJR algorithm is used to obtain the LLRs.

- Each user's LLRs are then used by a Soft Input Soft Output (SISO) decoder to deliver information for feeding back into the adaptive MAP multiuser detector.

Numerical Results

- A spreading gain of 7 is considered and a square-root raised cosine pulse is used for spreading.
- A rate 1/2 convolutional code with a constraint length of 3 is used to keep complexity low.
- The LMS algorithm is used to adaptively obtain the necessary parameters.

Effect of the number of training symbols

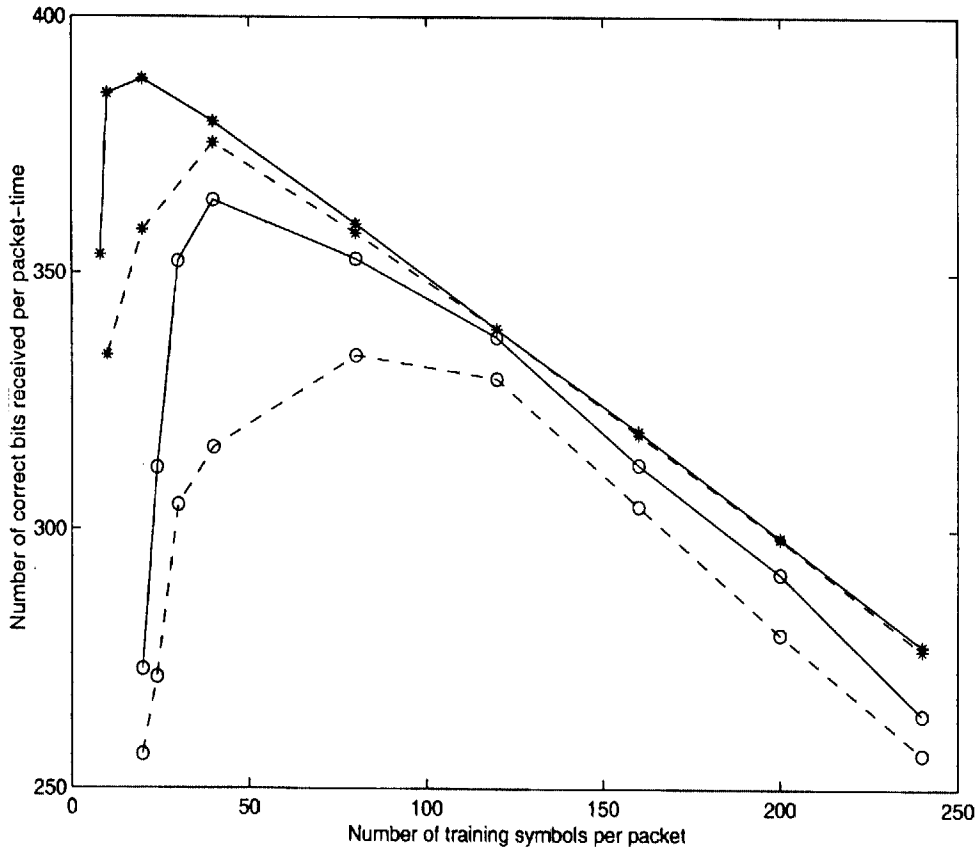

MMSE filter length

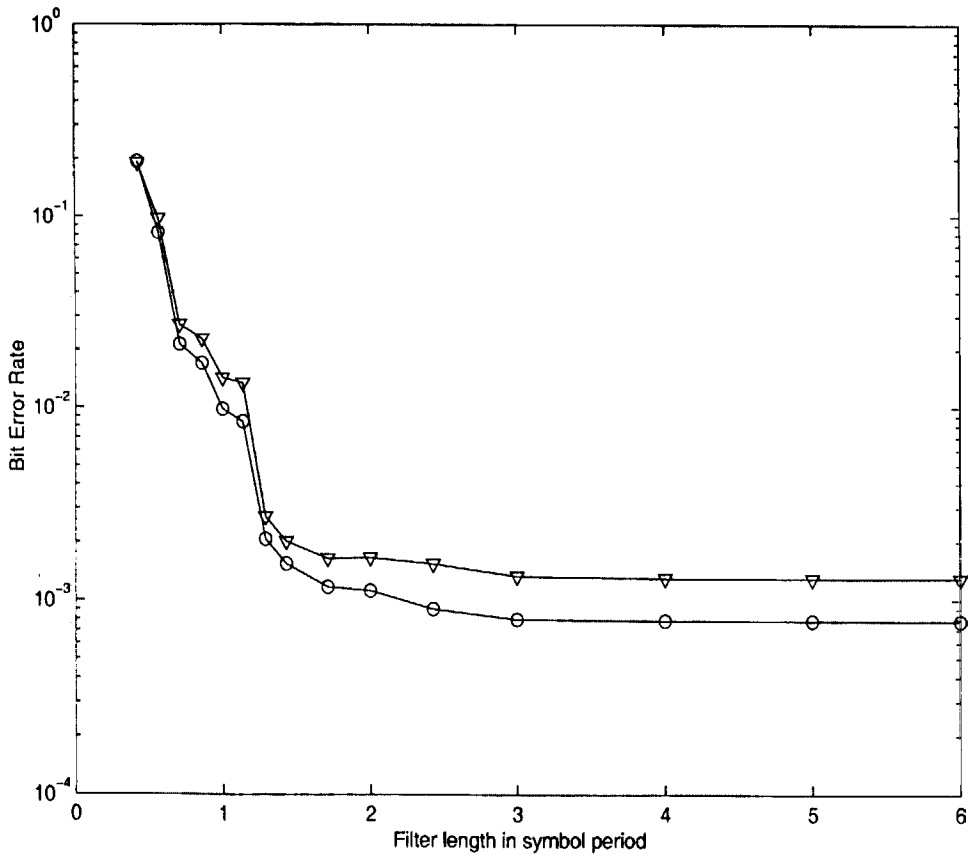

Adaptive and Wiener filtered turbo receiver

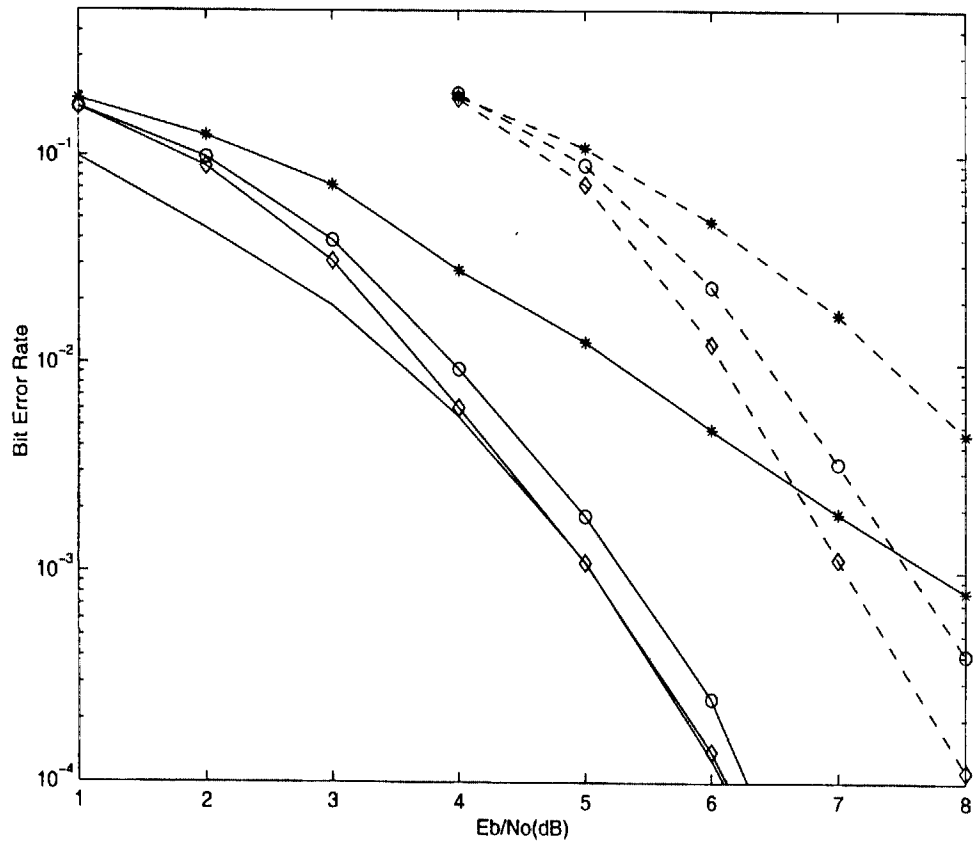

Performance in multicellular environment

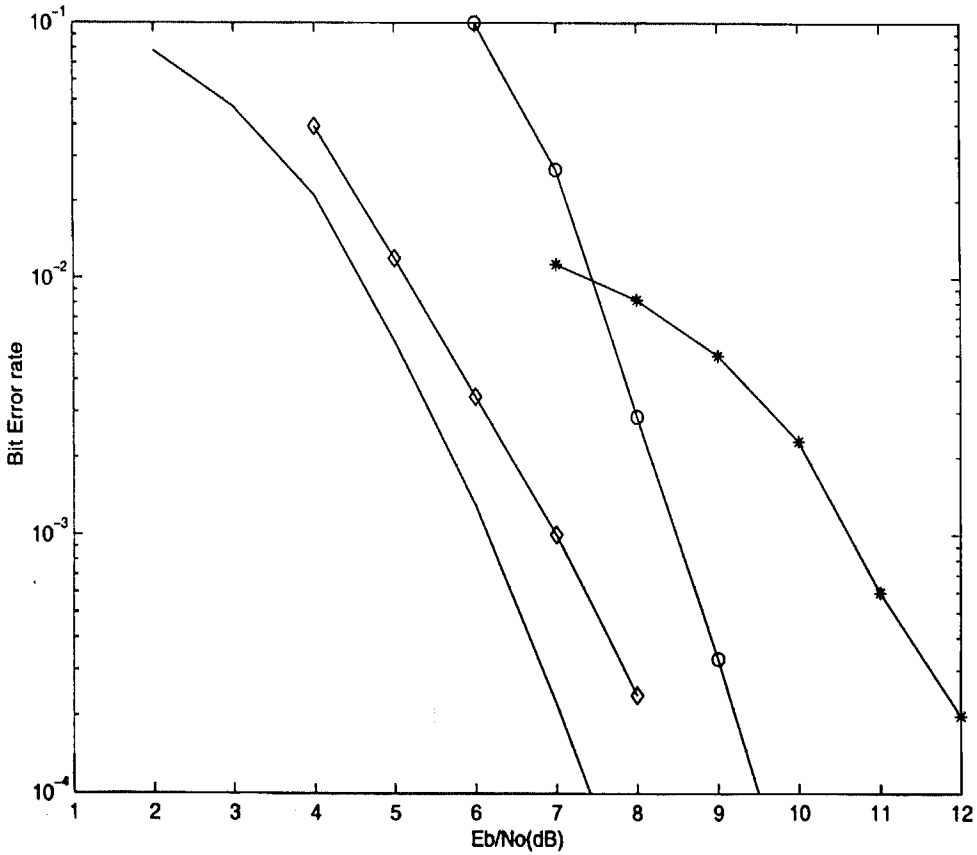

Comments on performance

- It is observed that by employing turbo detection, the number of training symbols required in each data packet can be significantly reduced. This improves effective data rate and provides guidelines for future packet design.
- Adaptive receivers without any *a priori* knowledge of the channel parameters can perform within a few dB of ideal single-user performance.
- Adaptive turbo receivers outperform fixed matched filter based turbo receivers when unknown interferers are present.

Possible Future Directions

- Efficient estimation of the signal-to-interference plus noise ratio and its effects on performance.
- Improvement on the convergence of the adaptive algorithm.
- Performance in the presence of narrowband communication channels.

Conclusions

- Two studies, namely a study on a bandwidth efficient modulation technique, and a study on turbo multiuser detection in spread spectrum systems, have been performed.
- The bandwidth efficient modulation technique, SPIK, is found to be highly bandwidth & power efficient in nonlinear channels.
- More work needs to be done to assess the performance of SPIK with sophisticated detectors and decoders (including performance in Ka band).
- The adaptive multiuser detector, in our study, is found to be highly successful. Its performance is close to single user's performance, and it can suppress undesired interferers.
- Future work will focus more on bandwidth efficient modulation studies.

A Decoupled Approach to Nonlinear ISI Compensation

Qingsong Wang and Raphael J. Lyman

Satellite Channel

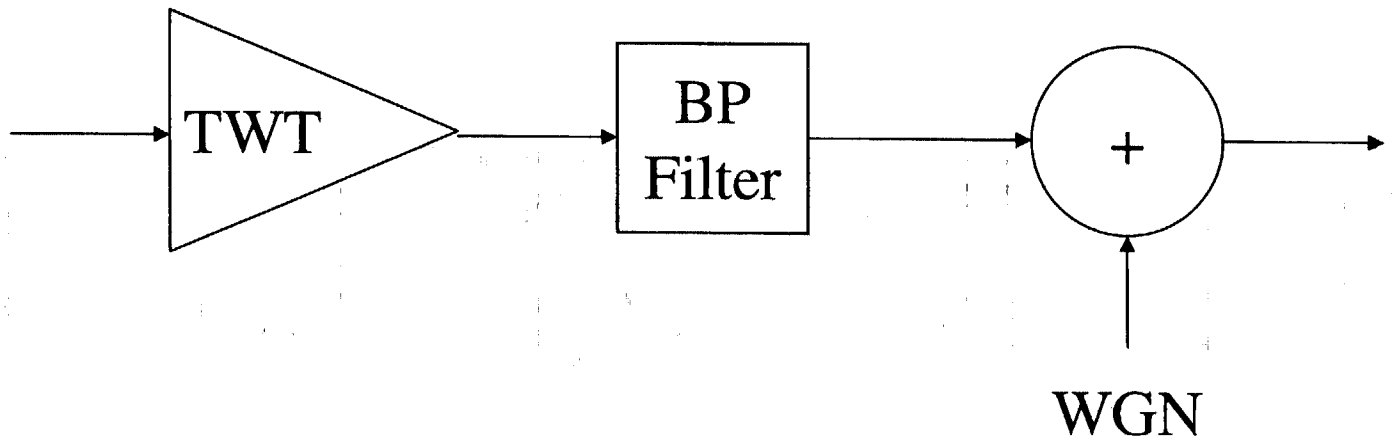

Nonlinear TWT Characteristic

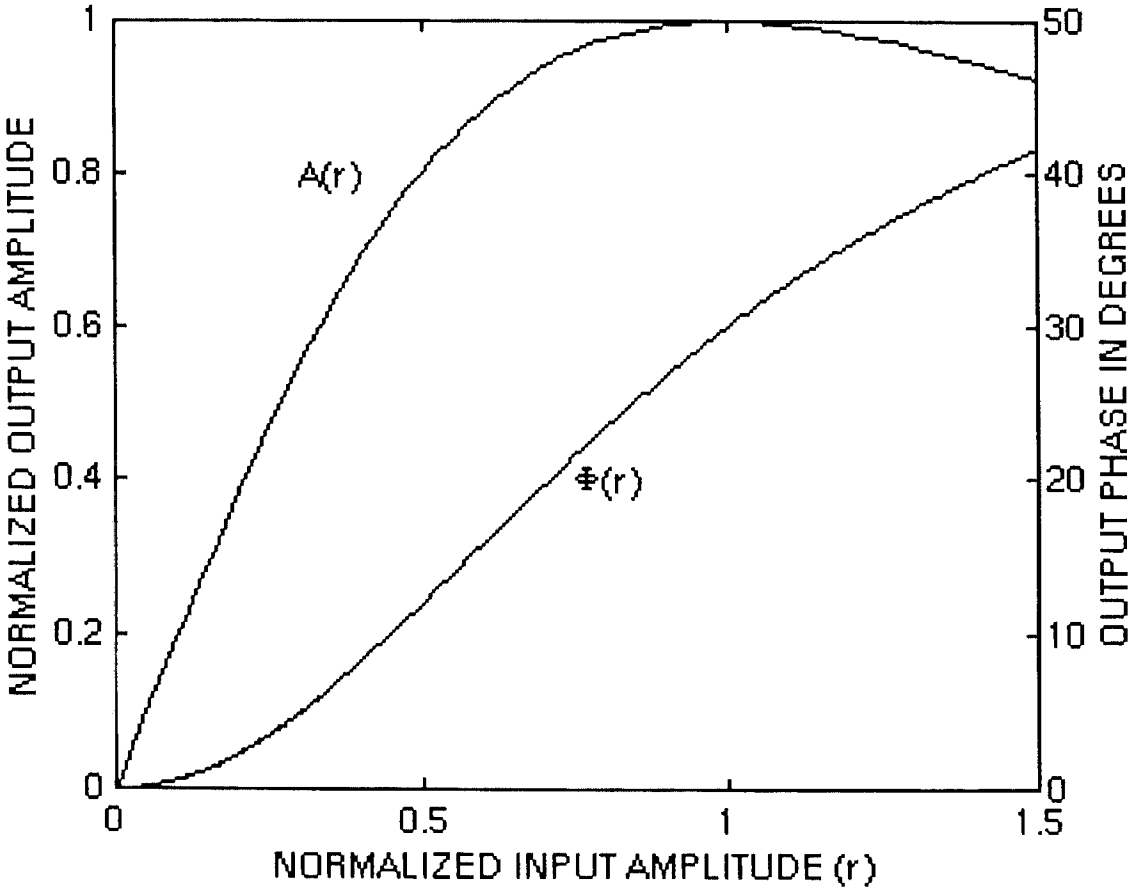

Received Signal

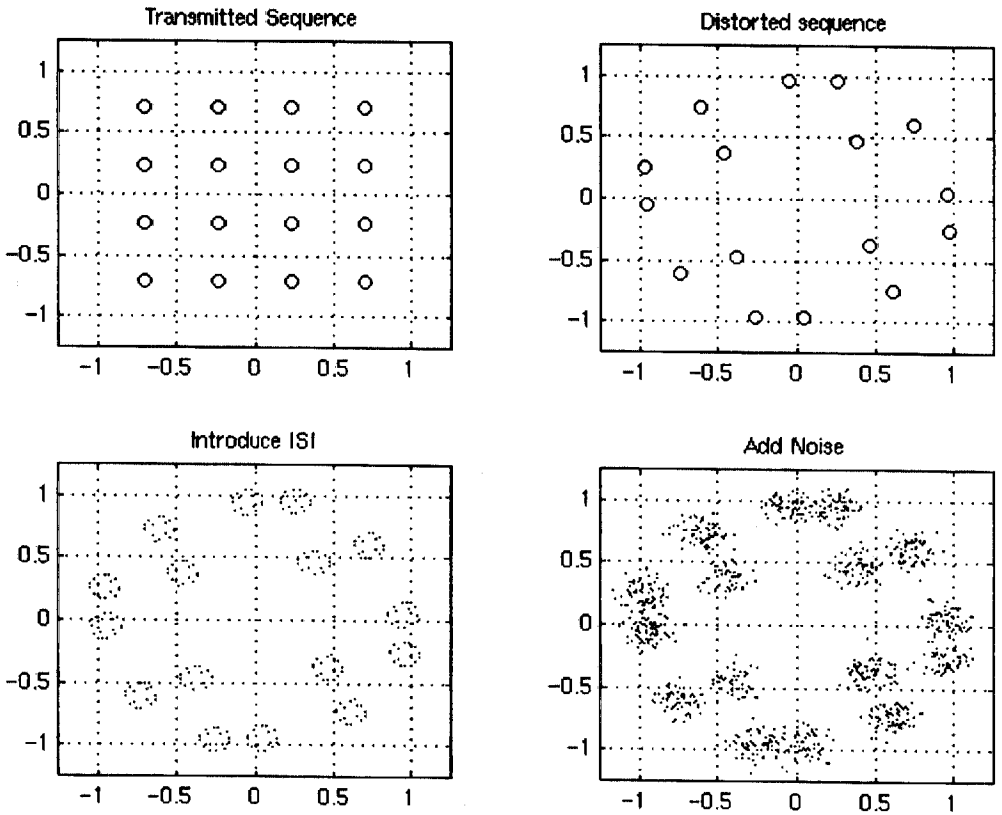

Previous Approaches

- TX based
  - Power Backoff
  - Predistortion
- RX based
  - Volterra Equalizer
  - Maximum-Likelihood Sequence Detection
- Trade off performance, complexity, power.

Our Approach

Decouple linearizer and equalizer.

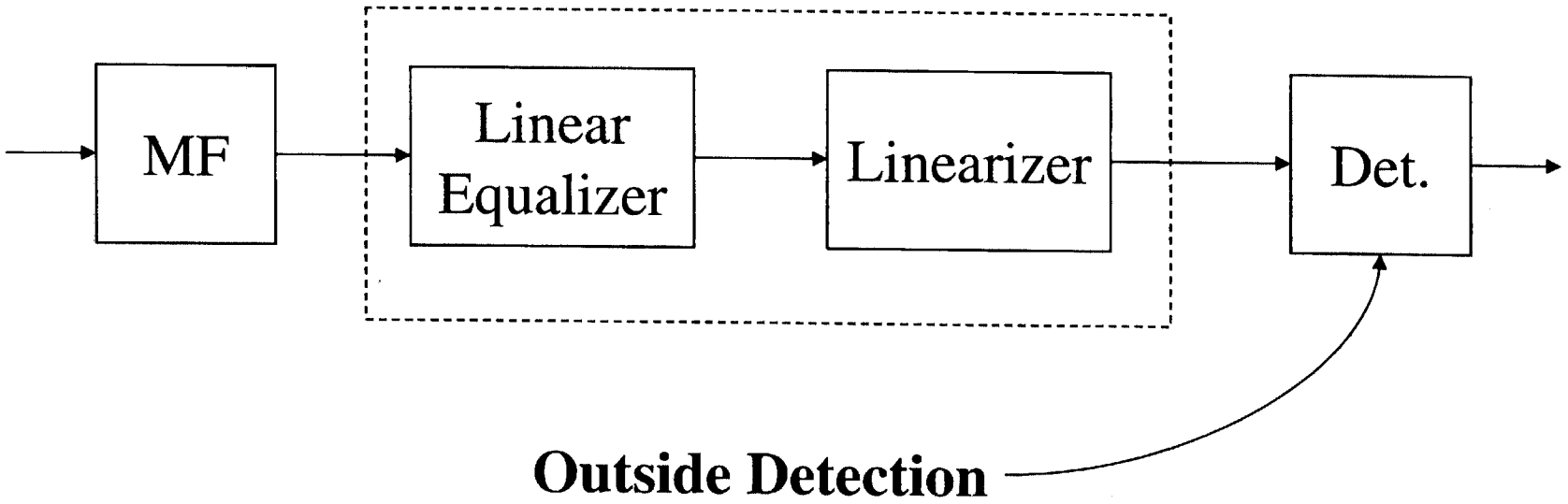

Outside Detection

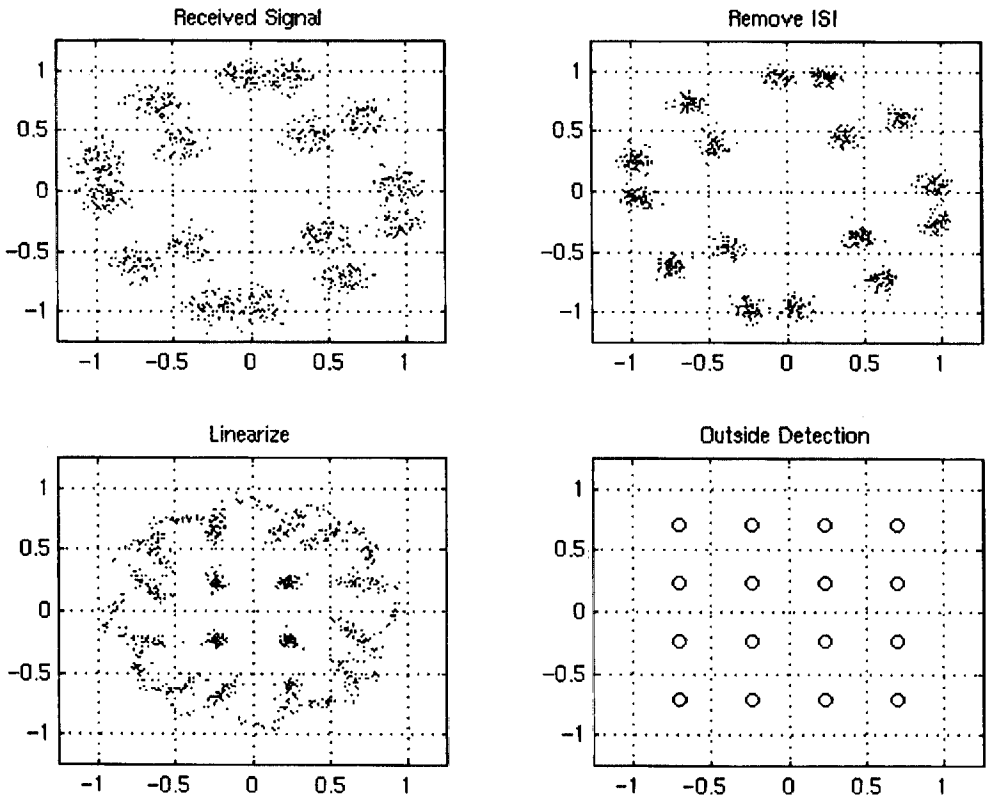

Noise Amplification

- Linearizer amplifies input noise.
- Switch position of linearizer and detector.

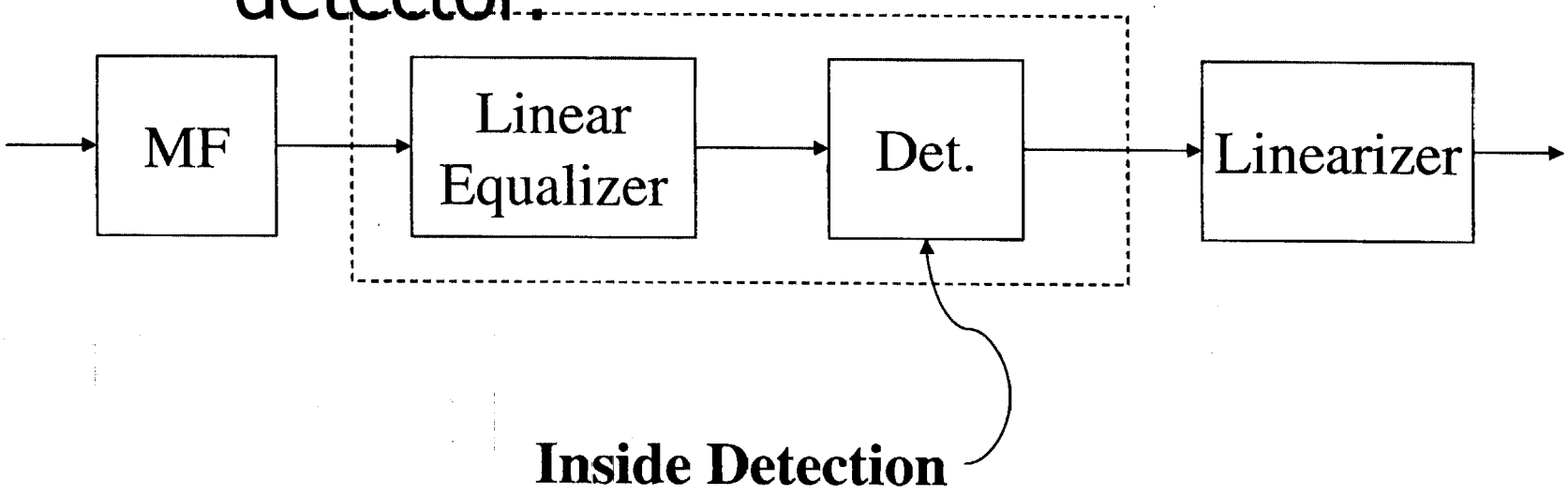

Inside Detection

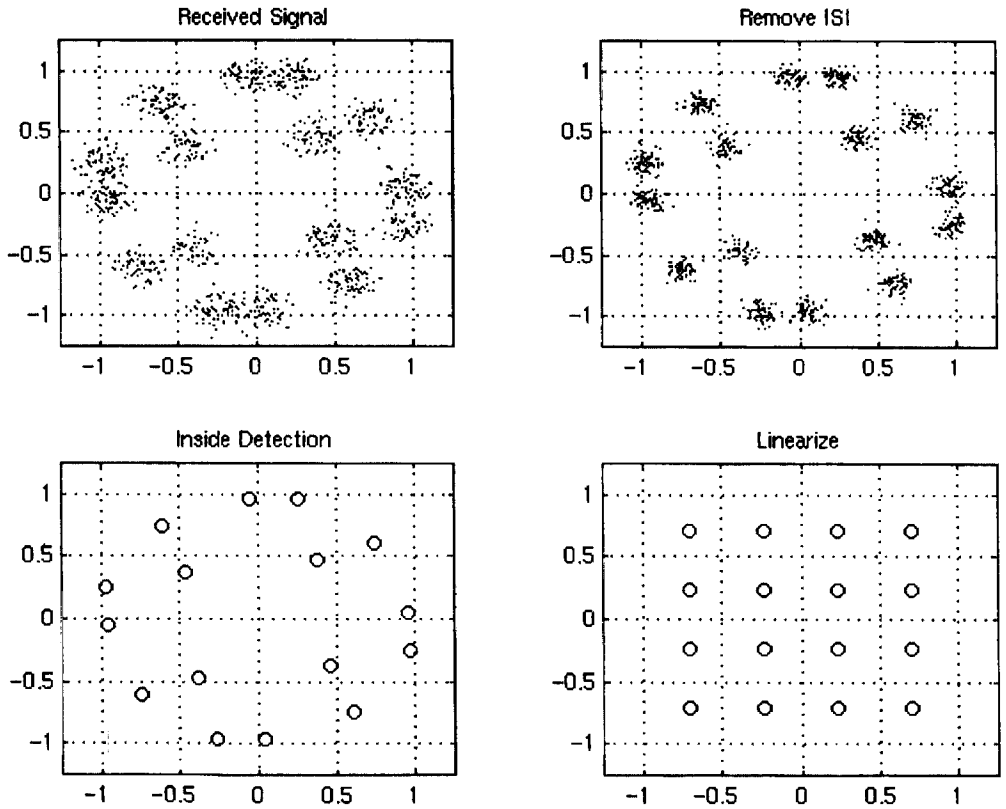

Bit Error Rate

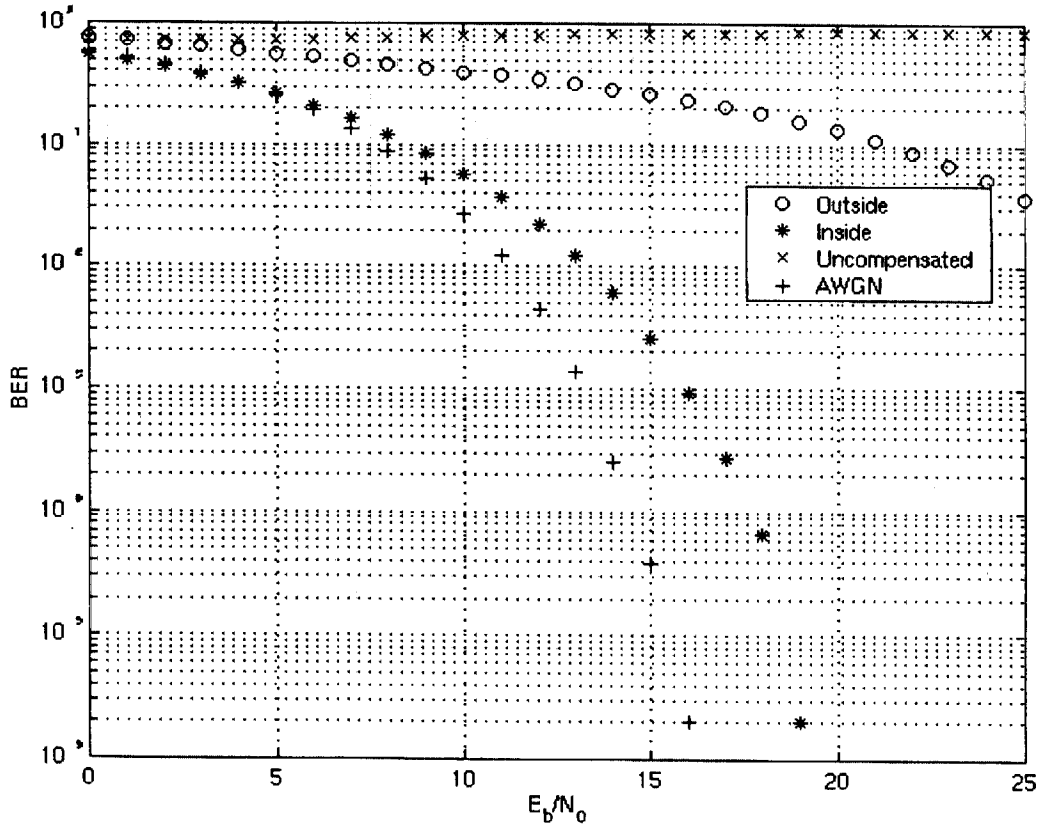

Conclusions

- Decoupling simpler than Volterra, MLSD.
- Inside detection offers near optimal performance.
- Need to study effects of pulse shaping.
- Comparison cases.

Space Internet Testing

Stephen Horan

Klipsch School of Electrical and Computer Engineering

New Mexico State University

Contents

- Simulator Upgrades
- SCPS vs. TCP Testing
- UDP-Based Testing

Simulator Upgrades

- Added link break capability to model link drop-outs
- Upgraded CPU to 1 GHz processor with more memory
- Upgrading serial interface speeds from 115 kbps to 965 kbps

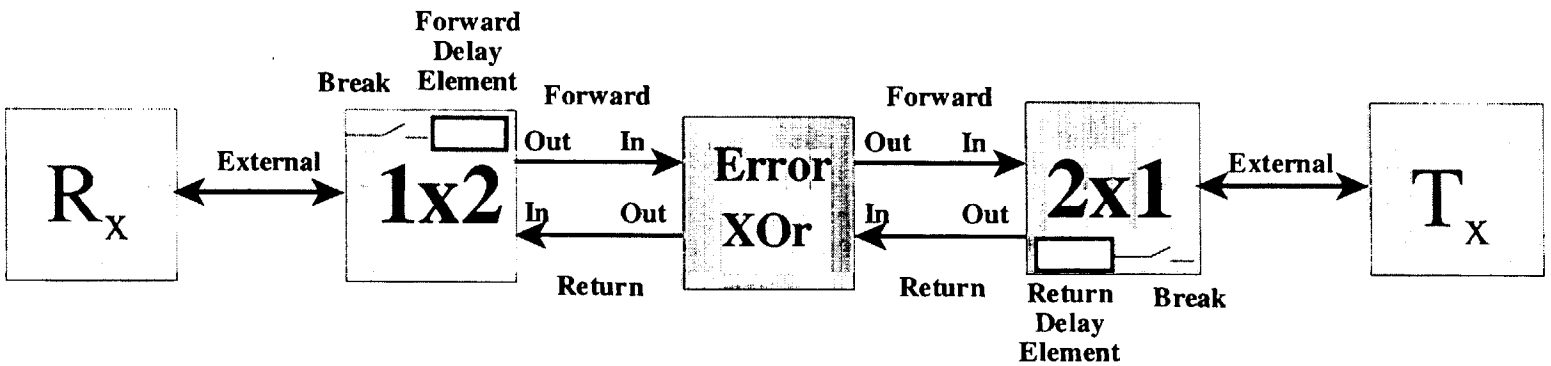

Simulator Upgrades

- The link break capability allows the user to separately control the break time and duration on the simulated forward and return links

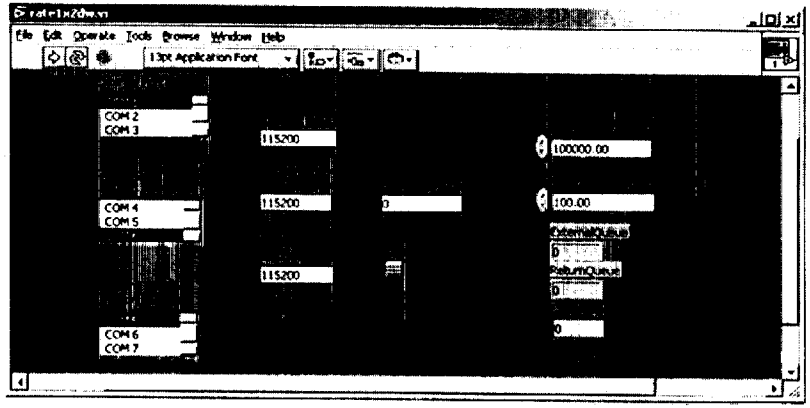

Simulator Upgrades

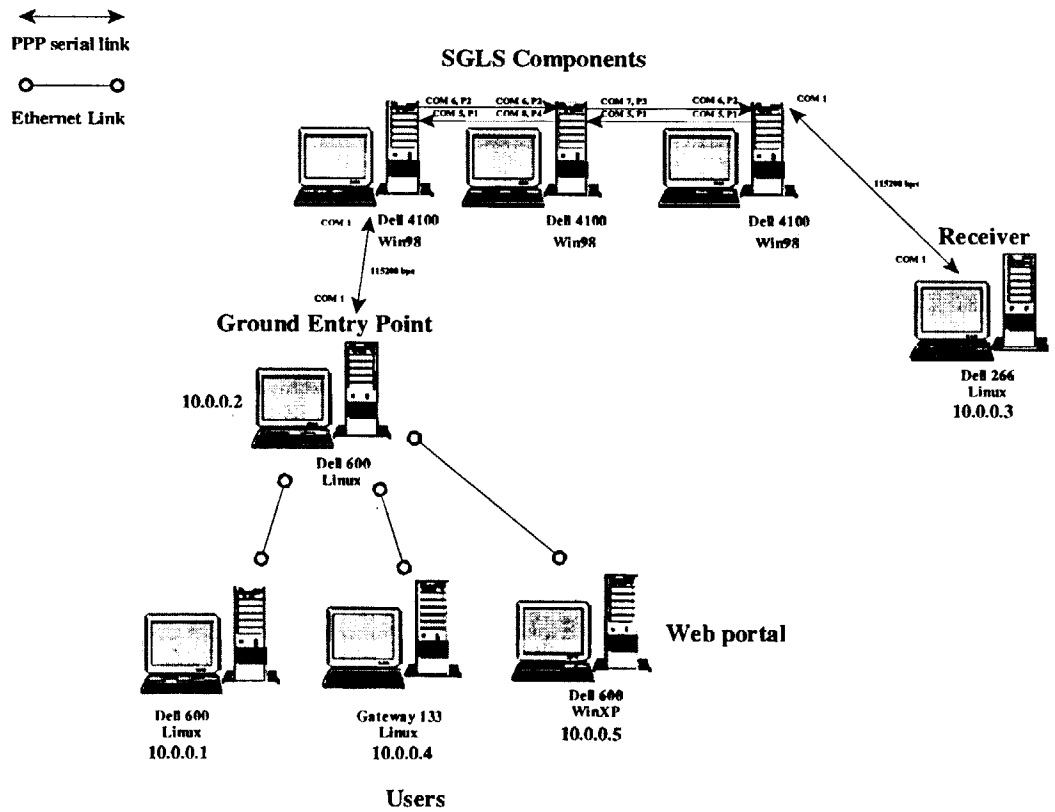

- Current simulator laboratory configuration
  - Linux and Windows-based user nodes
  - Channel Simulator (SGLS)
  - Linux-based satellite node

SCPS vs. TCP Testing

- Finished SCPS vs. TCP testing for the case of low bandwidth-delay product links
  - PhD awarded to Ruhai Wang based on this work
  - Performed a variety of tests to determine effects of channel BER, link delay, and protocol configuration on file throughput performance

Protocol Testing Results

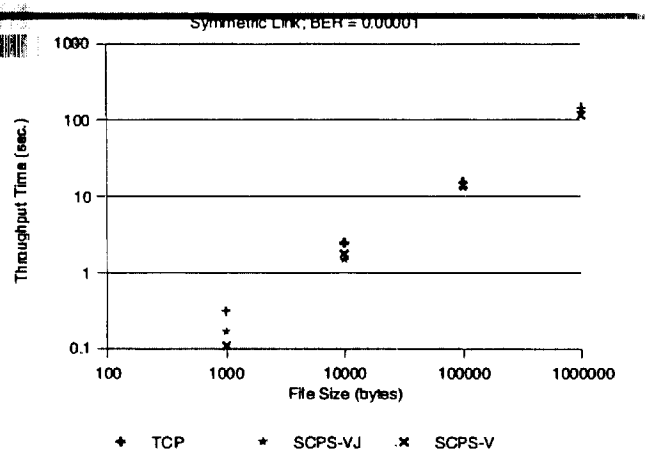

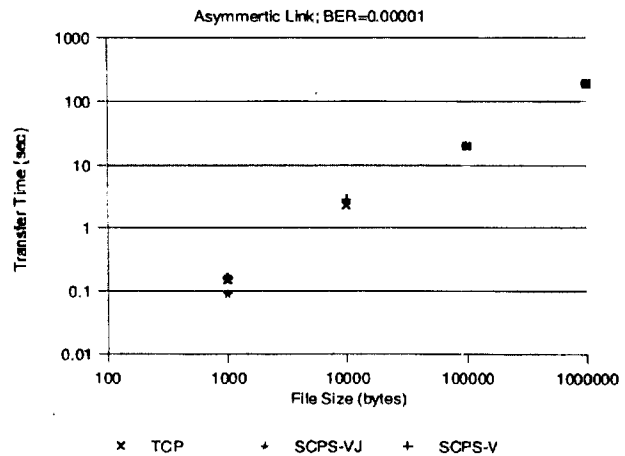

- For low bandwidth links (< 1 Mbps); GEO hops
  - no difference seen between TCP and SCPS for symmetric links (115 kbps/115 kbps)
  - almost no difference for asymmetric links (115kbps/2.4 kbps)
    - SCPS-VJ 10% better for large files with high BER
- Limited high-bandwidth testing (> 1 Mbps)
  - SCPS-VJ better than TCP/IP
  - TCP/IP better than SCPS-Vegas
  - Flow control algorithm sensitive

UDP-Based Testing

- As the next step in protocol testing, we are evaluating UDP-based techniques in a manner similar to that used for SCPS testing
  - Looking at a simple UDP transfer protocol and the MDP Protocol
  - UDP has the advantage of not using a "slow start" at the beginning and does not have an internal flow control that responds to channel errors
  - Both techniques use a Selective NAK to account for missing packets

UDP-Based Testing

- The Simple UDP has minimal overhead
  - Connection request and acknowledgment states
  - File Transfer State
  - Selective NAK accounting
- Comparing the data flow against a standard file transfer such as `ftp`.
- Results are just being determined now that the protocol developed and simulator upgrades at NMSU are complete

UDP-Based Testing

- MDP is an UDP-based protocol originally developed at the Navy Research Laboratory
- MDP is designed to support multicast and unicast transmissions
- Evaluation test suite is ongoing at the moment
  - Looking at how MDP compares with `ftp`
  - Looking at how MDP can be used to support multicast transmission from clusters of satellites
  - Looking at how MDP reacts to link outages

Optical Communications

Stephen Horan
Phillip DeLeon
Thomas Shay

Topics

- Overview
- Receiver Software Design
- Carrier Tracking Hardware
- Design Class
- Test Program

Overview

- The LOWCAL project was initiated with the goal of developing a flight hardware realization of the optical communications techniques
- A Hitchhiker flight request was submitted to NASA HQ
- Research team members have begun looking at a prototype of the flight hardware to see how this payload might be packaged and realized in actual components

Linux-Based Receiver for Lightweight Optical Communications without a Laser in Space

Philip Stanley and Phillip De Leon

December 2001

Overview

- LOWCAL system overview
- Receiver functions
- Communications format
- Receiver algorithm
- Software design and components
- Test procedure and results
- Performance analysis
- Conclusion

LOWCAL System Overview

- LOWCAL is a proposed laser-based, space-to-ground, communications system
  - Only minimal optical components are required in space (retroreflector, photodiodes, LCD modulator)
- LOWCAL presents a receiver with a carrier detect (CD) signal and an asynchronous binary signal (ABS) from which to determine data sequence

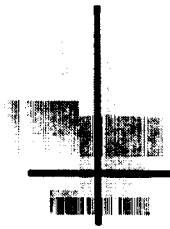

Receiver Functions

- Synchronize with transmitter
- Transform ABS into bit-stream
- Determine block boundaries and extract data
- Compare received bits to a known transmitted sequence and calculate BER
- Perform error detection and recovery
- Shift voltage levels to conform to RS-232, a common form of ABS

Design Assumptions

- Although link is two way, we assume the uplink and downlink are independent (no handshaking).
- Link duration is no longer than 5 minutes and may be interrupted due to atmospheric phenomena for up to 10 seconds
- All necessary hardware is already available in the flight computer (PC104 card with x86)-- we need only write software receiver codes

Communications Format

- In an asynchronous system, coordination between transmitter and receiver is necessary
- Data format

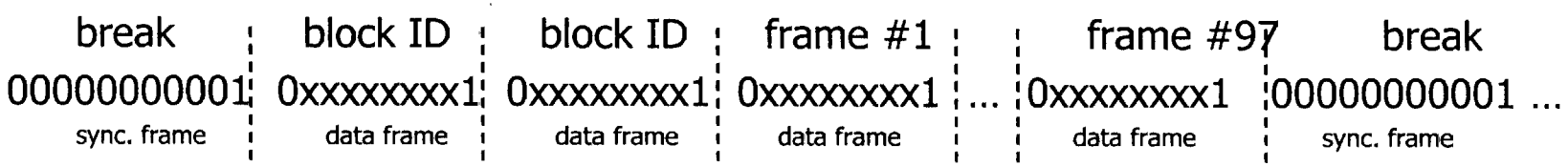

  - Synchronization is achieved with breaks which begin a "block"
  - Blocks are identified by a 16-bit integer starting at 0
  - Eight ID/data bits are packaged in a frame (with start/stop bits); 99 frames in a block

Bit Error Types

- "Data" Bit Errors
  - occur when any of the eight data bits inside a frame do not match predetermined bit sequence.
  - detected by user-space program.
- Framing Errors
  - occur when the stop bit of a frame is not a '1'.
  - detected by device.
  - receiver can always recover when these errors occur and produce accurate BER calculation(s).
- Block Errors
  - occur when block ID bits are obviously in error, e.g., current block ID <= last block ID + 1.
  - detected by user-space program.

Receiver Algorithm

init

wait for break

check previous block for errors

start new block

main loop

    get next frame

    if framing error

        go to *wait for break*

    else if carrier (CD) dropout

        loop until carrier is up

        go to *wait for break*

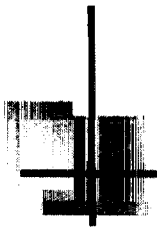

Receiver Algorithm (cont.)

```
    else if another break arrives
            check previous block for errors
            go to start new block
    else
            insert frame into block
end main loop
```

Software Design and Components

- There are two components to the receiver: 1) Linux device driver and 2) user-space program
- Device driver (Cereal)
  - responds to the data-ready interrupts, modem status interrupts, and line status interrupts
  - copies data from kernel-space to user-space when the user program calls `read()`
  - exists as two buffers in kernel-space

Software Design and Components (cont.)

- User-Space Program (Testrx)
  - Computes the BER of the link
  - Calls `read()`, requesting 99 bytes
  - Then compares received bytes with bytes in a file or bytes from FSR generator

Test Procedure and Results

- Three successively more rigorous tests were done to make sure software functioned correctly
- 10 minutes worth of FSR-generated data was sent to the receiver
  - 1st test: CD pin was asserted for the entire 10 minutes
  - 2nd test: the CD pin was toggled periodically
  - 3rd test: the CD pin was toggled randomly
- After ten minutes, the CD pin was de-asserted.
- All ten minutes worth of data was received without bit errors, and the receiver exited after 15 minutes.

Performance Analysis

- CPU Utilization
  - User-space program
    - It was found that program approached a CPU utilization of 0.6% after 5 minutes.
  - Cereal
    - It was found that the CPU utilization of the interrupt handler was 0.6%.

Conclusions

- A communications format and receiver were designed and implemented to recover data from the LOWCAL system and calculate BER
- Receiver uses existing flight computer and is composed of a Linux Device Driver and User program
- Receiver was rigorously tested
  - Realistic simulation of carrier detect and data signals shows the receiver can achieve synchronization with transmitter even with interruptions
- CPU utilization of receiver's software components is very low

Carrier Tracking Hardware

Tom Shay
Chris Garrett

Carrier Tracking Hardware

- A prototype circuit design for the FSK carrier tracking hardware was completed
- This design allows the receiver to determine the LOWCAL data transmission signal and becomes the input to the software to demodulate the data

Carrier Tracking Hardware

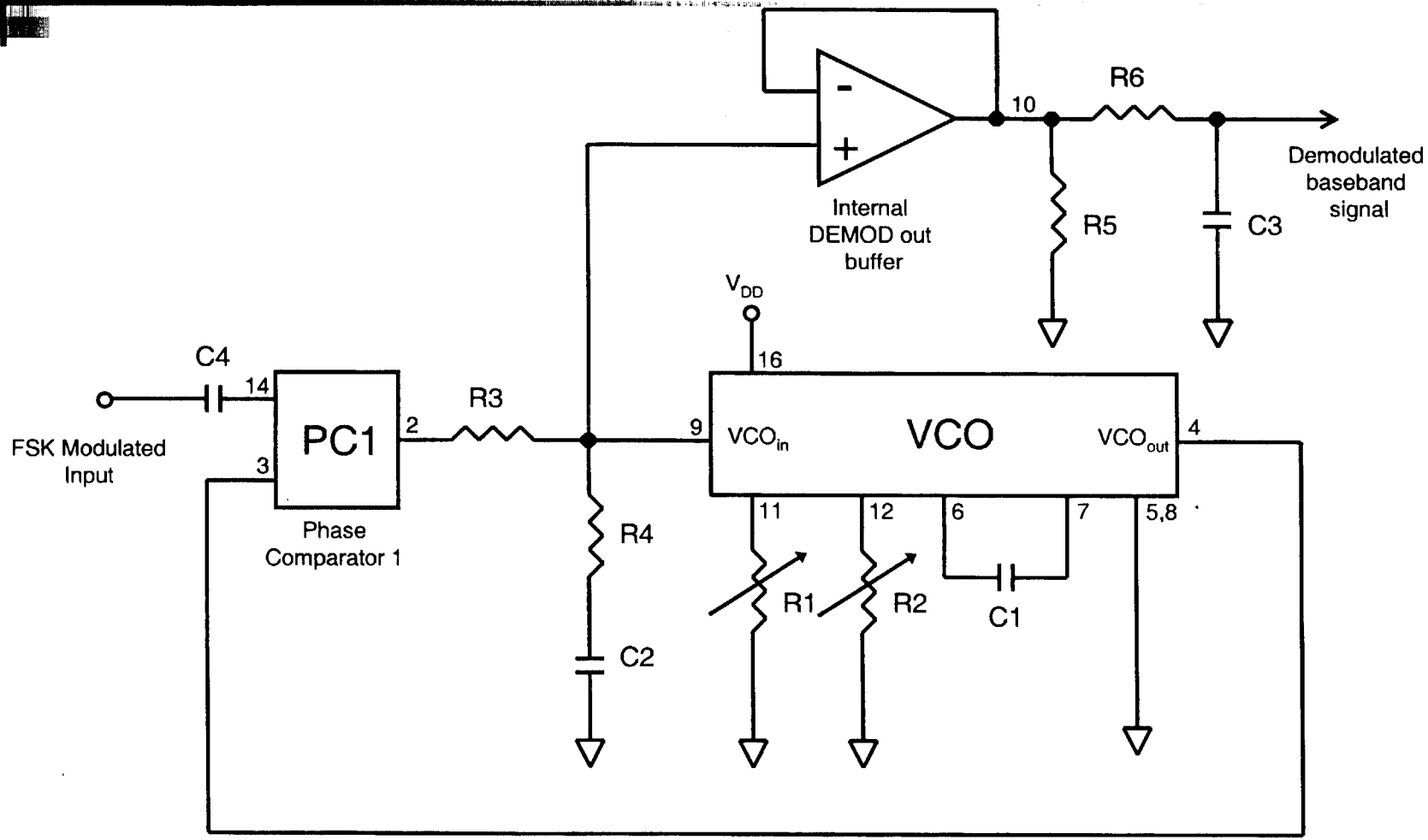

Design Class

Stephen Horan

Design Class

- A senior-level undergraduate class is being conducted during the 2001-2002 academic year to prototype how the hitchhiker design might be realized

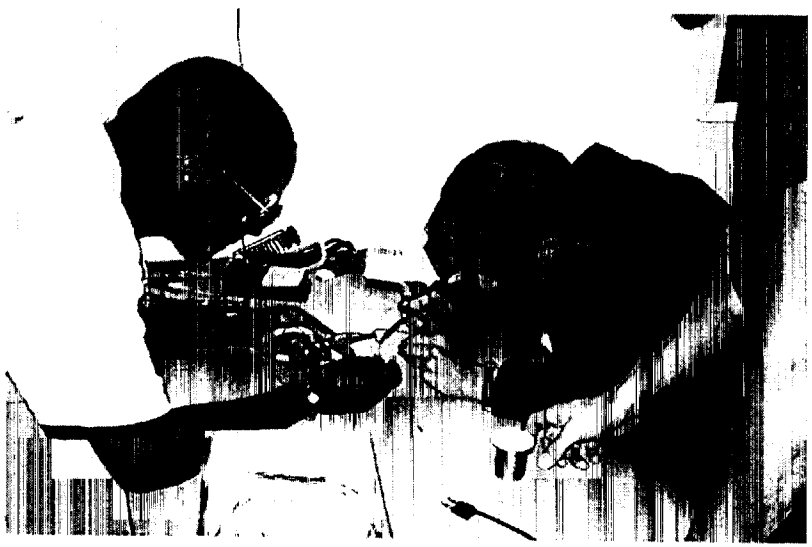

Students in senior design class

Design Class

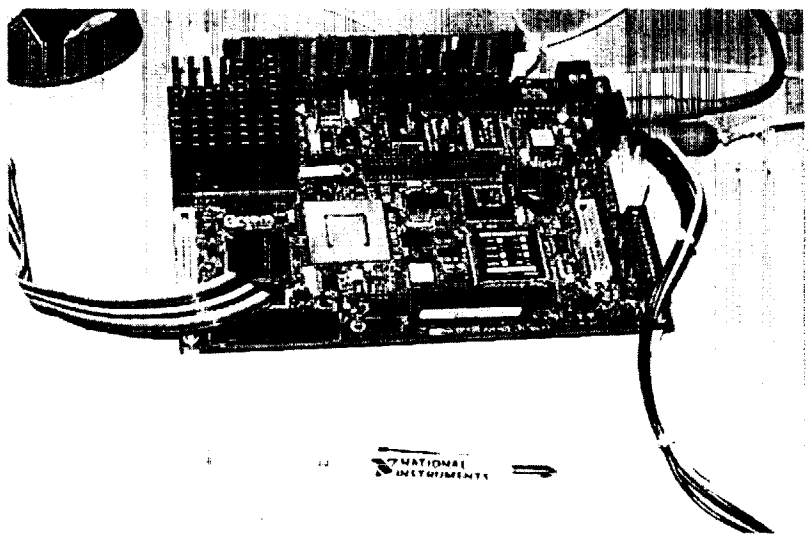

Linux-based single-board computer used for receiver development

- Class designing
  - Support interfaces to shuttle communications systems
  - Hitchhiker payload health and welfare telemetry
  - Data interfaces to optical experiments
  - Component packaging

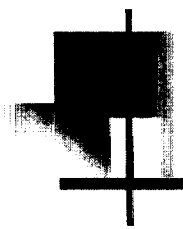

Test Program

Tom Shay

OPTICAL COMM PROGRESS

- UNM Atmospheric Test Range Facility Designed and is being assembled.
- The atmospheric test beam propagation systems have been designed and are being assembled.
- Automatic gain control circuit for the flight receiver has been designed and assembled and is being tested.
- The flight photoreceiver has been redesigned and is being assembled.
- A new FADOF is being assembled.
- A wide field-of-view flight retro-reflector has been assembled.
- UNM has written a joint proposal with Los Alamos National Lab to add a "Quantum Cryptography Experiment" to our flight experiment.
- Presented a paper at the Air Force Maui Optical Station Conference.
- Graduated 2 students with MS degrees.

Adaptive Spread Spectrum Receivers

Phillip DeLeon

Adaptive Spread Spectrum Receivers

- A prototype adaptive spread spectrum was completed using subband design techniques
- PhD was awarded to Stephan Berner based on this work

Subband Transforms for Adaptive Direct Sequence Spread Spectrum Receivers

Stephan Berner
Valence Semiconductor
26010 Mureau Rd.
Calabasas, CA 91361
sberner3@yahoo.com

Phillip De Leon
New Mexico State University
Klipsch School of Elect. and Comp. Eng.
Las Cruces, NM 88003
pdeleon@nmsu.edu

Abstract

Adaptive DSSS receivers have advantages over their fixed-matched filter counterparts including interference cancellation capabilities and simplification of PN code acquisition. However, convergence using an LMS algorithm may be too slow in situations with relatively high SNR. The use of a RLS algorithm will improve convergence speed but at significantly increased computational cost; fast RLS algorithms cannot be used because the filter is updated at the symbol rate rather than at every sample. In this paper, we examine subband receivers which utilize multiple, shorter length adaptive filters with the goal of speeding up convergence and reducing computation while maintaining equivalent BERs.

1 Introduction

Adaptive, Direct Sequence Spread Spectrum (DSSS) digital receivers have several advantages over their fixed matched-filter counterparts [1]. These advantages include the ability to minimize the effects of multiple-access (MA) interference, narrow band interference, and intersymbol interference (ISI) without having information about the channel or interferers. Another advantage of this receiver is that it requires no information about the PN code (other than its length) and thus does not require a code acquisition phase.

In the fractionally-spaced (FS) adaptive DSSS receiver illustrated in Fig. 1, a received baseband signal, $x(n)$ which is the sum of a desired component and interference, is passed through the adaptive filter, $\mathbf{w}$. The adaptive filter length, N, is equal to the PN code length times the number of samples per chip. The filter output is sampled at the symbol rate, T_s and compared with a known training sequence, $d(n)$. The resulting difference or error, $e(n)$ is used to adjust the filter coefficients. After a training period, the coefficient vector is an approximation of the pulse-shaped PN sequence (if the interference is moderate) and may be fixed or updated in decision-directed mode.

The input correlation matrix (assuming uncorrelated symbols), $\mathbf{R}$ is the outer product of the spreading sequence, $[s_1, s_2 \ldots s_L]^T$ with itself plus a diagonal matrix, $\sigma^2\mathbf{I}$ representing the zero mean, σ^2 variance, uncorrelated, additive white Gaussian noise (AWGN). Mathematically, the correlation matrix is given by

$$\mathbf{R} = \begin{bmatrix} s_1 \\ s_2 \\ \vdots \\ s_L \end{bmatrix} \begin{bmatrix} s_1 & s_2 & \ldots & s_L \end{bmatrix} + \sigma^2\mathbf{I}. \quad (1)$$

The eigenvalues of (1) are given by $\{s_1^2+s_2^2+\ldots+s_L^2+\sigma^2, \sigma^2, \ldots, \sigma^2\}$ and the eigenvalue spread is

$$\frac{\lambda_{max}}{\lambda_{min}} = \frac{s_1^2+s_2^2+\ldots+s_L^2+\sigma^2}{\sigma^2}. \quad (2)$$

The eigenvalue spread for such a matrix can be very large if the noise level is low; such ill-conditioning will lead to slow convergence of the LMS adaptive filter which can be a problem in a fast-changing environment. The use of a RLS algorithm will improve convergence speed but at significantly increased computational cost especially in the case of long PN codes; fast RLS algorithms cannot be used because the filter is updated at the symbol rate rather than at every sample [1].

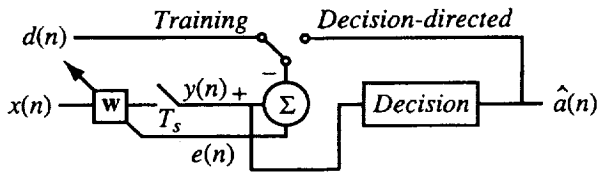

Figure 1: *Fractionally-spaced adaptive DSSS receiver.*

Subband and wavelet transforms have been previously applied to spread spectrum communications. A

notable overview of the applications are in [2]. In previous work, we proposed the subband, adaptive DSSS receiver in order to introduce parallelism into the architecture. Such parallelism could allow implementation of high-speed receivers using relatively low-speed digital hardware [3, 4]. As illustrated in Fig. 2, the received digitized baseband signal is decomposed by a linear transformation, $\mathbf{T}$ into M lower rate signals and adaptive filtering is performed in the subbands. The shorter adaptive filters have the potential to speed up convergence and reduce computation while maintaining equivalent bit error rates (BERs). Sampling at the symbol rate can be done in the subbands due to the assumption that the number of samples belonging to one symbol is a multiple of M. The subband signals are added after weighting by the gain factors $\alpha_1, \ldots, \alpha_M$ which can also be made adaptive in order to speed up convergence. Standard transforms such as DCT and Hadamard were used and performance (BER and convergence rates) was reported using simple LMS adaptive filters [4].

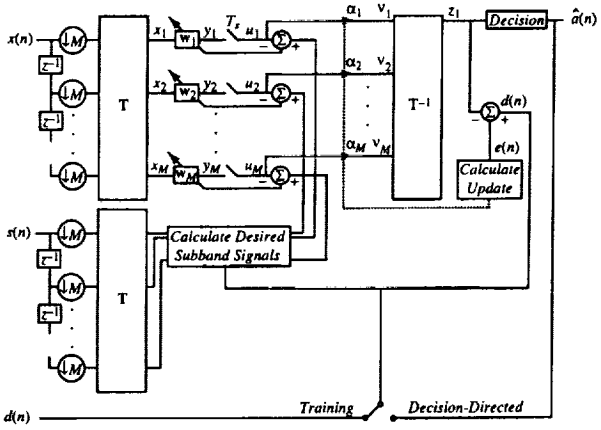

Figure 2: *Subband, adaptive DSSS receiver.*

In this paper, we further examine the subband, adaptive DSSS receiver with the focus being on the transform itself and how it effects the BER and convergence rate of the receiver.

2 Effect of the Subband Transform on Bit Error Rate

A common assumption about the error signal of an adaptive filter is that it is white gaussian noise after convergence of the filter [1]. Therefore the mean-squared error (MSE) after convergence is directly related to the BER. In order to understand the effect of the subband transform on BER, we could calculate the minimum MSE (MMSE) at the receiver output using a general transform and arbitrary input autocorrelations. As it turns out, the MMSE derived in this way is not too useful for purposes of optimizing the transform for minimum error, because it is a complicated rational function involving the elements of the transformation matrix [5]. Even for the simplest case (two subbands, length two subband filters), it is still difficult to work with.

As an alternative, we consider calculating a lower bound on the output signal-to-noise ratio (SNR) and designing $\mathbf{T}$ to maximize this bound. (Later in the paper, we will discuss the relation between maximizing the lower bound and the actual SNR.) Here, we assume additive, white gaussian noise (AWGN) with variance σ^2 but no interference. The derivation is presented for the case of a two subband receiver with length two subband filters—other cases can be easily generalized for arbitrary parameters. We refer the reader to Fig. 2 for notation used in this section.

In order to simplify the analysis, we assume the gain factors are fixed. We denote L as the number of samples per symbol, and assume $N = L/M$ is an integer. Next, we define

$$\mathbf{X} = \begin{bmatrix} \mathbf{x}_1 & \mathbf{x}_2 & \ldots & \mathbf{x}_M \end{bmatrix} = \begin{bmatrix} x_{11} & x_{12} & \ldots & x_{1M} \\ x_{21} & x_{22} & \ldots & x_{2M} \\ \vdots & \vdots & \vdots & \vdots \\ x_{N1} & x_{N2} & \ldots & x_{NM} \end{bmatrix} \quad (3)$$

as the $N \times M$ matrix whose columns are vectors of subband (transformed) samples with

$$x_{ij} = \sum_{m=1}^{M} t_{jm} x\left(m + (i-1)M\right) \quad (4)$$

where x is the received input signal and t_{ij} is the i,jth element of $\mathbf{T}$. We define

$$\mathbf{W} = \begin{bmatrix} \mathbf{w}_1 & \mathbf{w}_2 & \ldots & \mathbf{w}_M \end{bmatrix} \quad (5)$$

as the matrix whose columns are the coefficient vectors of the adaptive subband filters. The oversampled and pulse shaped spreading sequence, s is partitioned into vectors of length M which form the columns of

$$\mathbf{S} = \begin{bmatrix} s_1 & s_{M+1} & \ldots & s_{(N-1)M+1} \\ s_2 & s_{M+2} & \ldots & s_{(N-1)M+2} \\ \vdots & \vdots & \vdots & \vdots \\ s_M & s_{2M} & \ldots & s_{NM} \end{bmatrix}. \quad (6)$$

The subband version of the spreading sequence is given by

$$\mathbf{S}_{\text{sub}} = (\mathbf{TS})^T$$

$$= \left[\begin{array}{cccc} \mathbf{S}_{s1} & \mathbf{S}_{s2} & \dots & \mathbf{S}_{sM} \end{array} \right]$$

$$= \left[\begin{array}{cccc} S_{s11} & S_{s12} & \dots & S_{s1M} \\ S_{s21} & S_{s22} & \dots & S_{s2M} \\ \vdots & \vdots & \vdots & \vdots \\ S_{sN1} & S_{sN2} & \dots & S_{sNM} \end{array} \right]. \quad (7)$$

The signal power at the receiver output (after the rightmost summation in Fig. 2) is given by

$$P_s = \left[\left(\mathbf{S}_{s1}^T \mathbf{S}_{s1} \right) \alpha_1 a + \left(\mathbf{S}_{s2}^T \mathbf{S}_{s2} \right) \alpha_2 a \right]^2 \quad (8)$$

where $\mathbf{S}_{si}$ is the subband version of the oversampled pulse shaped spreading sequence defined in (7) and a is the data bit (either $+1$ or -1). The noise power, assuming that the noise outputs of the subbands are independent (true if the rows of $\mathbf{T}$ are orthogonal), is given by

$$P_n = \left(\mathbf{S}_{s1}^T \mathbf{S}_{s1} \right) \sigma^2 \left(t_{11}^2 + t_{12}^2 \right) \alpha_1^2 + \left(\mathbf{S}_{s2}^T \mathbf{S}_{s2} \right) \sigma^2 \left(t_{21}^2 + t_{22}^2 \right) \alpha_2^2. \quad (9)$$

The output SNR is then the ratio of (8) to (9)

$$\mathrm{SNR} = \frac{P_s}{P_n} \quad (10)$$

$$= \frac{\left[\left(\mathbf{S}_{s1}^T \mathbf{S}_{s1} \right) \alpha_1 a + \left(\mathbf{S}_{s2}^T \mathbf{S}_{s2} \right) \alpha_2 a \right]^2}{\sigma^2 \left[\left(\mathbf{S}_{s1}^T \mathbf{S}_{s1} \right) \left(t_{11}^2 + t_{12}^2 \right) \alpha_1^2 + \left(\mathbf{S}_{s2}^T \mathbf{S}_{s2} \right) \left(t_{21}^2 + t_{22}^2 \right) \alpha_2^2 \right]}.$$

Calculating the gradient of (10) with respect to the entries of $\mathbf{T}$, t_{ij} leads to a system of nonlinear equations which is difficult to solve. Therefore some simplification of the problem is necessary.

We assume that the absolute value of all elements of the oversampled pulse shaped spreading sequence and all elements of $\mathbf{T}$ are smaller or equal 1. Then $\mathbf{S}_{si}^T \mathbf{S}_{si} \leq 8$ and

$$\mathrm{SNR} \geq \frac{\left[\left(\mathbf{S}_{s1}^T \mathbf{S}_{s1} \right) \alpha_1 a + \left(\mathbf{S}_{s2}^T \mathbf{S}_{s2} \right) \alpha_2 a \right]^2}{8\sigma^2 \left[\left(t_{11}^2 + t_{12}^2 \right) \alpha_1^2 + \left(t_{21}^2 + t_{22}^2 \right) \alpha_2^2 \right]}. \quad (11)$$

The problem is now to maximize this lower bound.

If we constrain the denominator in (11) to be

$$\left(t_{11}^2 + t_{12}^2 \right) \alpha_1^2 + \left(t_{21}^2 + t_{22}^2 \right) \alpha_2^2 = k \quad (12)$$

where k is a constant, then we need only maximize the numerator. Because the data is assumed to be binary, the square can be dropped in order to find the extrema. Using the method of Lagrange multipliers, leads to the following eigenvalue problem

$$\left[\begin{array}{cc} 2\alpha_1^2 \mathbf{A}_1 & 0 \\ 0 & 2\alpha_1^2 \mathbf{A}_2 \end{array} \right] \left[\begin{array}{c} t_{11} \\ t_{12} \\ t_{21} \\ t_{22} \end{array} \right] = \mathbf{0} \quad (13)$$

where

$$\mathbf{A}_i = \left[\begin{array}{cc} \frac{s_1^2 + s_3^2}{\alpha_i} - \lambda & \frac{s_1 s_2 + s_3 s_4}{\alpha_i} \\ \frac{s_1 s_2 + s_3 s_4}{\alpha_i} & \frac{s_2^2 + s_4^2}{\alpha_i} - \lambda \end{array} \right]. \quad (14)$$

Since the submatrices, $\mathbf{A}_1$ and $\mathbf{A}_2$ in (13) are identical except for the factors α_1, α_2, the eigenvectors of

$$\mathbf{B} = \left[\begin{array}{cc} s_1^2 + s_3^2 & s_1 s_2 + s_3 s_4 \\ s_1 s_2 + s_3 s_4 & s_2^2 + s_4^2 \end{array} \right] \quad (15)$$

solve the optimization problem and yield $\mathbf{T}$. For the general case of M subbands with subband filter length N, the entries of $\mathbf{B}$ are given by

$$b_{mn} = \sum_{i=1}^{M} s_{(i-1)M+m} s_{(i-1)M+n}. \quad (16)$$

The algorithm for finding the optimal transformation matrix can be summarized as follows. Build the matrix $\mathbf{B}$ with entries as in (16) using the spreading sequence which is assumed to be given. Find the eigenvectors of $\mathbf{B}$ and use them as the rows of $\mathbf{T}$ (in any order).

One open question is the relation between the lower bound of the output SNR, which was maximized, and the true SNR. A numerical evaluation of the exact SNR equation (10) for different matrices reveals that the matrix $\mathbf{T}$, optimized with the method above leads to the maximum SNR value. It should be noted that all orthonormal matrices also lead to the same maximum SNR value, but the theory for why this happens is beyond the scope of this paper. For more details see [5].

While in theory all orthonormal matrices lead to the maximum SNR, simulation results (shown below) demonstrate that the optimized transform performs slightly better than other standard transforms (DCT, Hadamard, Identity) which are also (scaled) orthonormal matrices. The main reason is the fact that the SNR maximization was done assuming a matched filter, however an adaptive filter converges to the Wiener solution. Another reason is the additional noise each adaptive filter creates because the tap vector is wandering around the optimal solution. Therefore it is better, regarding the output SNR, to concentrate the signal energy into as few subbands as possible (which is what is ultimately happening with the optimal transform) while the subband filters containing no signal energy adapt to the zero vector. This feature may be exploited to reduce computation in subbands with little or no signal energy.

The BER performance of the proposed subband, adaptive DSSS receiver was simulated and compared to theory, the matched filter (MF) receiver, and the fullband adaptive DSSS receiver. These results are

shown in Fig. 3 and illustrate that the optimal transform is slightly better than the standard transforms. System parameters include a length 31 PN sequence, chip pulses shaped with a square-root raised cosine (SRRC) filter (50% excess bandwidth), and a NLMS adaptive algorithm; we assume perfect carrier and chip synchronization. For each simulation point, 2×10^5 symbols are used, the MSE curves are averaged over 100 simulation runs. In addition, we assume four other users (MA interference) and three narrowband interferences (sinusoids), each 6dB stronger than the desired signal; zero mean, white Gaussian noise is also added to achieve a desired SNR which during training is 6dB. In the fullband receiver, the adaptive filter length is 128 (length 31 PN sequence, four samples per chip which yields 124 samples, resampled to get 128 samples). In the subband receiver, we use $M = 4$ subbands with a subband adaptive filter length of 32.

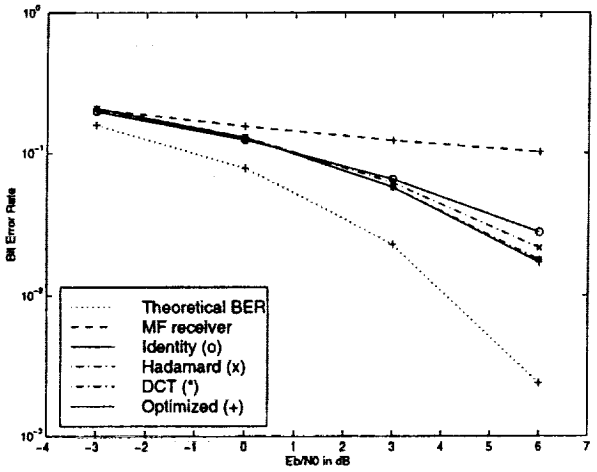

Figure 3: *Bit error rate for the subband receiver using various transforms.*

3 Eigenvalue and Convergence Analysis with LMS/NLMS Filters

In this section, we investigate how $\mathbf{T}$ effects the eigenvalue spread of the autocorrelation matrices of the subbands. As is known, this determines the convergence speed of the LMS/NLMS subband adaptive filters [6].

3.1 Desired User in AWGN

As described earlier, the autocorrelation matrix of the received signal is given by (1). The subband autocorrelation matrices are also outer products plus AWGN. For the case of two subbands and length two subband filters, the autocorrelation matrix of the first subband is

$$\mathbf{R}_{11} = \begin{bmatrix} \rho_1^2 & \rho_1\rho_3 \\ \rho_1\rho_3 & \rho_1^2 \end{bmatrix} + \sigma^2 \left(t_{11}^2 + t_{12}^2\right) \mathbf{I} \quad (17)$$

where

$$\begin{aligned} \rho_1 &= (t_{11}s_1 + t_{12}s_2) \\ \rho_3 &= (t_{11}s_3 + t_{12}s_4)\,. \end{aligned} \quad (18)$$

The eigenvalue spread of subband 1 is then

$$\frac{\lambda_{\max}}{\lambda_{\min}} = \frac{\rho_1^2 + \rho_3^2 + \sigma^2\left(t_{11}^2 + t_{12}^2\right)}{\sigma^2\left(t_{11}^2 + t_{12}^2\right)}. \quad (19)$$

This expression shows that designing $\mathbf{T}$ to minimize the eigenvalue spread in subband 1 (and thus speed up convergence in LMS/NLMS case) is in conflict with maximizing the output SNR in subband 1 since

$$\rho_1^2 + \rho_3^2 = \mathbf{s}_1^T\mathbf{s}_1, \quad (20)$$

appears also in the numerator of the SNR as in (10). This is, of course, a measure of the signal energy in subband 1. To see this conflict another way, for maximum SNR in subband 1, the first row of $\mathbf{T}$, $[t_{11}\ t_{12}]$, should be correlated with the oversampled, pulse-shaped spreading sequence, $s_1, \ldots, s_4$, as much as possible. For minimum eigenvalue spread in subband 1, $[t_{11}\ t_{12}]$ needs to be orthogonal to the spreading sequence and thus in direct contrast to maximizing the SNR of subband 1.

Based on the results of Section 2, however, a reasonable tradeoff between receiver convergence time and SNR performance is possible by distributing the signal energy as uniformly as possible between the subbands. As a side note, we can show in the case of Multiuser Interference that simultaneous maximization of the subband SNR and minimization of the subband eigenvalue spread is also not possible. However, as above, a reasonable tradeoff can be made between receiver convergence time and BER performance with appropriate choice of transform.

3.2 RLS Subband Adaptive Filters

The results in the previous section demonstrate that a subband transform for the adaptive DSSS receiver cannot be designed to improve the convergence speed of the LMS/NLMS filters while maintaining good BER (which is the ultimate goal). The situation is different if the RLS algorithm is used because the convergence speed of this algorithm depends on the filter length unlike that of LMS/NLMS algorithms which depend on the eigenvalue spread of the input correlation matrix. Of course the price paid for RLS's fast convergence is increased computation (proportional to the square of

the filter length). Fig. 4 shows the BER of the fullband receiver as well as for the subband receiver (using a DCT) with four and eight subbands using RLS filters, under the same interference conditions as in the previous section. The scaling factor of the initial correlation matrix of the RLS algorithm provides some possibility to trade final MSE value for convergence (found during experiments), however it is difficult to adjust the final MSE to the same value as the fullband receiver. Therefore the receivers are compared with final MSE values and BERs not exactly equal. Comparison of convergence times of the fullband and subband adaptive receivers is based on the similar BER performance, e.g. the BER of the fullband receiver was adjusted by varying parameters in the RLS algorithm until it was approximately the same as the BER for the subband receiver. Then convergence time was then measured by how long it takes the MSE to come within 1dB of the steady-state value. Table 1 summarizes the simulation results along with the matched filter receiver and theoretical results. As seen from Table 1, the proposed subband receiver has a BER performance comparable to the fullband receiver. With $M = 8$ subbands, there is a slight degradation in BER (but still better than the matched filter receiver) due to losses associated with the higher-dimension decomposition. However, as expected when using the RLS algorithm, we achieve faster convergence with the shorter length filters.

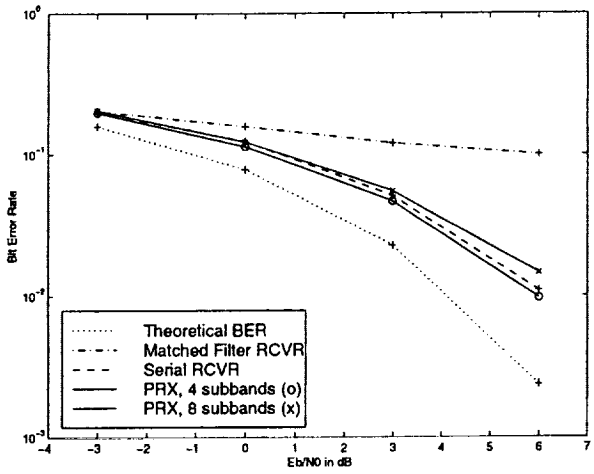

Figure 4: *Bit error rate for the subband receiver with RLS adaptive filters.*

4 Conclusions

In this paper, we have carefully analyzed the transform used in a proposed subband, adaptive DSSS receiver with the goal of improving BERs, convergence speed, and computational complexity. Our work shows that while an optimal transform can be designed to improve (slightly) BERs compared to standard transforms, it cannot improve convergence when using subband LMS/NLMS adaptive filters. However, when used with subband RLS adaptive filters, both convergence speed and computational complexity can be improved.

Table 1: Performance of Subband, Adaptive RLS DSSS Receiver.

Number of Subbands	*BER for Various SNRs*			*Conv. Time*
	0dB	3dB	6dB	
Theoretical	0.0880	0.027	0.0030	N/A
MF Receiver	0.1558	0.1210	0.0999	N/A
1 (Fullband)	0.1237	0.0515	0.0109	150 Sym
4	0.1140	0.0471	0.0097	100 Sym
8	0.1232	0.0556	0.0146	50 Sym

Acknowledgment

The authors wish to acknowledge the support of this research by NASA, Grant #NAG 5-9323.

References

[1] S. Miller, "An adaptive direct-sequence code-division multiple-access receiver for multiuser interference rejection," *IEEE Trans. Comm.*, pp. 1746–1754, Feb./Mar./Apr. 1995.

[2] A. Akansu and M. Smith, eds., *Subband and wavelet transforms: design and applications*, Kluwer Academic Publishers, Norwell, MA., 1996.

[3] D. Raphaeli, R. Sadr, P. P. Vaidyanathan, and S. Hinedi, "Parallel digital modem using multirate digital filter banks," *JPL Publication*, , no. 20, 1994.

[4] S. Berner and P. De Leon, "Parallel digital architectures for high-speed adaptive dsss receivers," *Proc. 34th Asilomar Conf. Signals, Syst., Comput.*, 2000.

[5] S. Berner, "Subband transforms for adaptive direct sequence spread spectrum receivers with application to parallel implementations," *Ph.D. Dissertation, New Mexico State University*, 2001.

[6] S. Haykin, *Adaptive Filter Theory*, Prentice-Hall, Englewood-Cliffs, N.J., 3 edition, 1998.